scientific reports

Check for updates

OPEN

Exploring the nexus between hydroclimatic variability, population growth, land use land cover change, and long-term upper Nyong Basin River chemistry (Central Africa rainforest)

David Eric Komba[1]✉, Gustave Raoul Nkoue Ndondo[1], Jean Riotte[2,3], Stéphane Audry[2,3]✉, Bertil Nlend[1], Bernadette Nka Nnomo[3,4], Suzanne Ngo Boum-Nkot[1], Henriette Ateba Bessa[3,4], Enoh Jeanot Fongoh[1,4], Laurie Boithias[2], Christelle Lagane[2], Jules Rémy Ndam Ngoupayou[3,5], Marie Joseph Ntamak-Nida[1], Jacques Etame[1] & Jean Jacques Braun[2,3]

Hydrological and hydrogeochemical functioning of rivers depends on the relationship between climatic variability, land use and land cover change (LULCC), and population dynamics. However, there is a Central Africa.
this gap by examining the link between hydroclimatic variability, population growth, LULCC, and river water chemistry in the upper Nyong basin (UNB). Atmospheric temperature and rainfall data were obtained from Climatic Research Unit gridded Time Series 4.07 (CRU TS 4.07), in Google Earth Pro 7 software. Demographic data were obtained by projection based on the 1976, 1987 and 2005 censuses, assuming population increase as in the past. Land use and land cover (LULC) maps for 2005–2020 periods were produced from Landsat images (Landsat 7 ETM + from 2005 to 2010 and Landsat 8 OLI from 2015 to 2020). elihood Algorithm was used to classify the Landsat images in ArcGIS 10.8 Software. Three LULC classes (Forest, impervious and agricultural surface and water) were suc curacies from 96.4 to 100%, and Kappa The study also used 29-year (1994–2023) meteorological (rainfall), hydrological (discharge) and hydrochemical (water temperature [WT], pH, electrical conductivity (EC), alkalinity [Alk], Na^+, K^+, Ca^{2+}, Mg^{2+}, NO_3^-, SO_4^{2-}, F^-, Cl^-, HCO_3^-, dissolved organic carbon [DOC], silica [SiO_2] and suspended particulate matter [SPM]) database provided by Multiscale TROPIcal CatchmentS critical zone observatory (M-TROPICS CZO) in the UNB. The results show that population increased in UNB from 2.6 million to 4.1 million between 2005 and 2020. This population growth has increased demands for food, housing, agricultural activities, etc. To meet these demands, the populations have converted 1,207 km^2 of forest into impervious and agricultural surface (buildings, roads, agricultural land, etc.). More so, LULC classes have evolved from 2005 to 2020 as follows: 17,845 km^2 to 16,638 km^2 (-6.7%) for forest, 1,376 km^2 to 2,587 km^2 (+88%) for impervious and agricultural surface, and 15 km^2 to 11 km^2 (-26.7%) for water. The increase in
$p < 0.01$) in pH, EC, TDS, cation and NO_3^- concentrations were observed. This increase was attributed to the discharge of household and industrial waste and wastewater into the environment and river, and probably due to a greater contribution of groundwater to surface water. The groundwater contribution was supported
$p <$
in Cl^-, SO_4^{2-}, Alk, HCO_3^-, and SiO_2 is associated with increased photosynthetic activity due to

eutrophication of the Nyong River, as well as the long term soil depletion of these chemical elements by slash-and-burn agriculture.

Keywords Land use and land cover change, Population growth, River water chemistry, Upper Nyong basin, Tropical ecosystems

[1]Faculty of Sciences, University of Douala, P.O Box 24157, Douala, Cameroon. [2]GET, Université de Toulouse, CNRS, IRD, UPS, Toulouse, France. [3]International Joint Laboratory DYCOFAC, IRGM-UY1-IRD, Yaounde, Cameroon. [4]Research Centre for Water and Climate Change (CRECC), Institute of Geological and Mining Research (IRGM), Yaounde, Cameroon. [5]Department of Earth Sciences, University of Yaounde I, Yaounde, Cameroon. ✉email: koderic@live.fr; stephane.audry@get.omp.eu

Sub-Saharan Africa records the fastest population growth rate in the world, estimated at more than 2 $\%.y^{-1}$ [1]. This rapid population growth generates multiple demands such as: housing, food, economic activities, transport, etc. Thus, there is a profound and rapid transformation of land use and land cover (LULC), notably deforestation in favor of impervious and agricultural surface (roads, urbanization, agricultural land, bare soil)[2–5]. It is worthnoting that impervious surface increases runoff, erosion and sedimentary deposits in rivers[6]. These sedimentary deposits lead to rapid filling of the riverbed and high eutrophication. The aquatic plants that develop accelerate the filling of the bed, slow down the flow of rivers. Despite this rapid increase in population and the subsequent growth in impervious and agricultural surface, cities in Sub-Saharan Africa do not have waste and wastewater management systems. The ever-increasing waste and wastewater generated by the population, agricultural activities, urban runoff (soil leaching and remobilization within drains) and various industries is dumped, without control or prior treatment, into the environment and into rivers, constituting a serious threat. This threat is also accompanied by the effect of climate, particularly in tropical areas.

In tropical basins, long-term discharge variation mainly depends on climate change and/or land use and land cover change (LULCC)[7–11]. Climatic factors include rainfall and ambient temperature[6,12–17]. When the influence of climate change plays a role, an increase in rainfall and/or decrease in ambient temperature lead to increase flow, and vice versa. Furthermore, LULCC can result in an increase in impervious and agricultural surface (agricultural land, urban surface, etc.) and a decrease in forest area[14]. Transition of tropical forest to impervious and agricultural surface increase surface runoff through factors such as decrease infiltration and interception, and significant decrease evapotranspiration and groundwater recharge[11]. Agriculture increases surface runoff by promoting the formation of impermeable soil crust, and due to low cover at the beginning of the rainy season[18–21]. In addition, factor such as water withdrawal for various uses (drinking water, irrigation, etc.) influences the river hydrology in the long term[22,23]. The increasing demand for water withdrawal and diversion is one of the major anthropogenic causes for the decreasing water discharge of the river[22]. In the long term, the combination of hydroclimatic and anthropogenic factors (LULCC) contribute to river chemistry evolution.

The evolution of solute concentrations in river water over the long term depends on hydroclimatic variability (discharge), groundwater contribution to surface water and/or anthropogenic factors, including LULCC[22,24–27]. In general, increase in discharge, decrease in groundwater contribution to surface water and/or decrease anthropogenic impact lead to a significant decrease in physicochemical parameters, and concentrations of cations and anions[25,28–30]. On the other hand, the decrease in discharge, the increase in the contribution of groundwater to surface water and/or the increase in anthropogenic impact can lead to a significant increase in physicochemical parameters, and concentrations of cations and anions. The established interaction between hydroclimatic variability and LULCC and their impact on river chemistry is an interesting topic to explore in the humid tropical zone of Central Africa.

In humid tropical Central Africa sub-region, there are no studies investigating the link between hydroclimatic variability and LULCC and their impact on river chemistry. Some existing studies link climate variability and variation in river flow[31]sometimes taking into account LULCC[32–34]. Other studies focus mainly on LULCC[35–37]. The failure to consider river chemistry lies in the almost complete absence of a long-term hydrochemical record that could allow for long-term studies. Furthermore, population growth was not taken into account in these studies which is considered the main driver of LULCC in Africa[2,38,39]. More so, population growth and an increase in impervious and agricultural surface deteriorate river water quality through increasing production of waste and wastewater[35,40–44].

The upper Nyong basin (UNB), located in southern Cameroon, provides an interesting specific framework for relating hydroclimatic variability, LULCC, population growth and river water chemistry. This is related to the rapid changes observed in the basin and certain characteristics likely to induce a change in the chemical composition of the Nyong River. These characteristics include: the presence of a vast wetland upstream of the basin, which is rich in organic matter and exploited for rice cultivation, the degradation of more than 90% of primary forest into secondary forest, vast plantations in development, and constantly expanding cities. In addition, the Nyong basin is one of the four monitoring setups of a long-term monitoring program called Service National d'Observation Multiscale TROPIcal CatchmentS (SNO M-TROPICS; https://mtropics.obs-mip.fr/), and located in the tropical zone. As part of this program, meteorological, hydrological (discharge) and hydrochemical (water temperature [WT], pH, electrical conductivity (EC), alkalinity [Alk], Na^+, K^+, Ca^{2+}, Mg^{2+}, NO_3^-, SO_4^{2-}, F^-, Cl^-, HCO_3^-, dissolved organic carbon [DOC], silica [SiO_2] and suspended particulate matter [SPM]) database have been made available for the Nyong basin since 1994. Such data offer the advantage of examining the variation of the chemical composition of the river in response to environmental changes over the long term. Based on the hydrochemical database, climatic data (atmospheric temperature and rainfall), Landsat imagery and population census data, this study aims to investigate the link between hydroclimatic variability, LULCC,

population growth and river water chemistry in the UNB. Firstly, the study examines the long-term evolution of the following components: climatic parameters (ambient temperature and rainfall), the discharge and chemical composition of the river, LULCC, and population trends. Secondly, it deduces the link that exists between these components based on their relative evolutions.

Study area

This study focuses on the UNB, which lies between longitudes 09°54'E-13°30'E and latitudes 2°48'N-4°40'N (Fig. 1) in South Cameroon. It covers an area of 19,240 km^2. The UNB is under an equatorial climate with 4 seasons of unequal importance[45]. The main rainy season (autumn) lasts from September to November, and the main dry season (winter) lasts from December to March. The short rainy (spring) and dry (summer) seasons extend respectively from April to June and from July to August. Rainfall generally decreases from the West (near the coast) to the East (towards the continent) of the basin[46]. From a value of 1638 mm in Mbalmayo, the rainfall decreases to 1598 mm in Yaounde, and to 1449 mm in Ayos[46,47]). The average relative humidity is 84% and evapotranspiration in Yaounde is estimated at 1235 $mm.y^{-1}$[47]. The vegetation consists of semi-deciduous forest[48] and the dominant soils are ferralitic and hydromorphic[49,50]).

Geomorphologically, the UNB is located on the southern Cameroonian plateau which has an average altitude of 700 m, constituting one of the main characteristic geomorphological features of southern Cameroon. The slopes are extremely low (0.05 to 0.15‰)[46]. The relief is generally very little contrasted and the limits of the basin are only exceptionally higher than 700 m (Fig. 1).

Geologically, the UNB is covered by four geological entities constituting parts of the Pan-African Chain of Central Africa (represented by the Yaounde Group) and the Congo Craton (represented by the Ntem Complex): (1) Yaounde series, (2) Ayos-Mbalmayo-Beng-Bis series, (3) Ntem unit and (4) Nyong unit. The Yaounde series consists of metasedimentary and metaigneous rocks[51–54]. The Ayos-Mbalmayo-Bengbis series is made up of four facies: chlorite mica schists, aluminous mica schists, muscovite quartzites and chlorite quartzites[55]. The Nyong unit comprises four petrographic groups: (i) metavolcanic sedimentary rocks, probably remnants of greenstone belts, with orthopyroxene gneisses, garnet-rich amphibole-pyroxenites and associated gneisses, banded iron formations and mafic-ultramafic metavolcanic rocks; (ii) migmatitic gray gneiss with tonalite–trondhjemite–granodiorite (TTG) composition; (iii) syn- to late-tectonic charnockite, (grano)dioritic augengneisses, granite

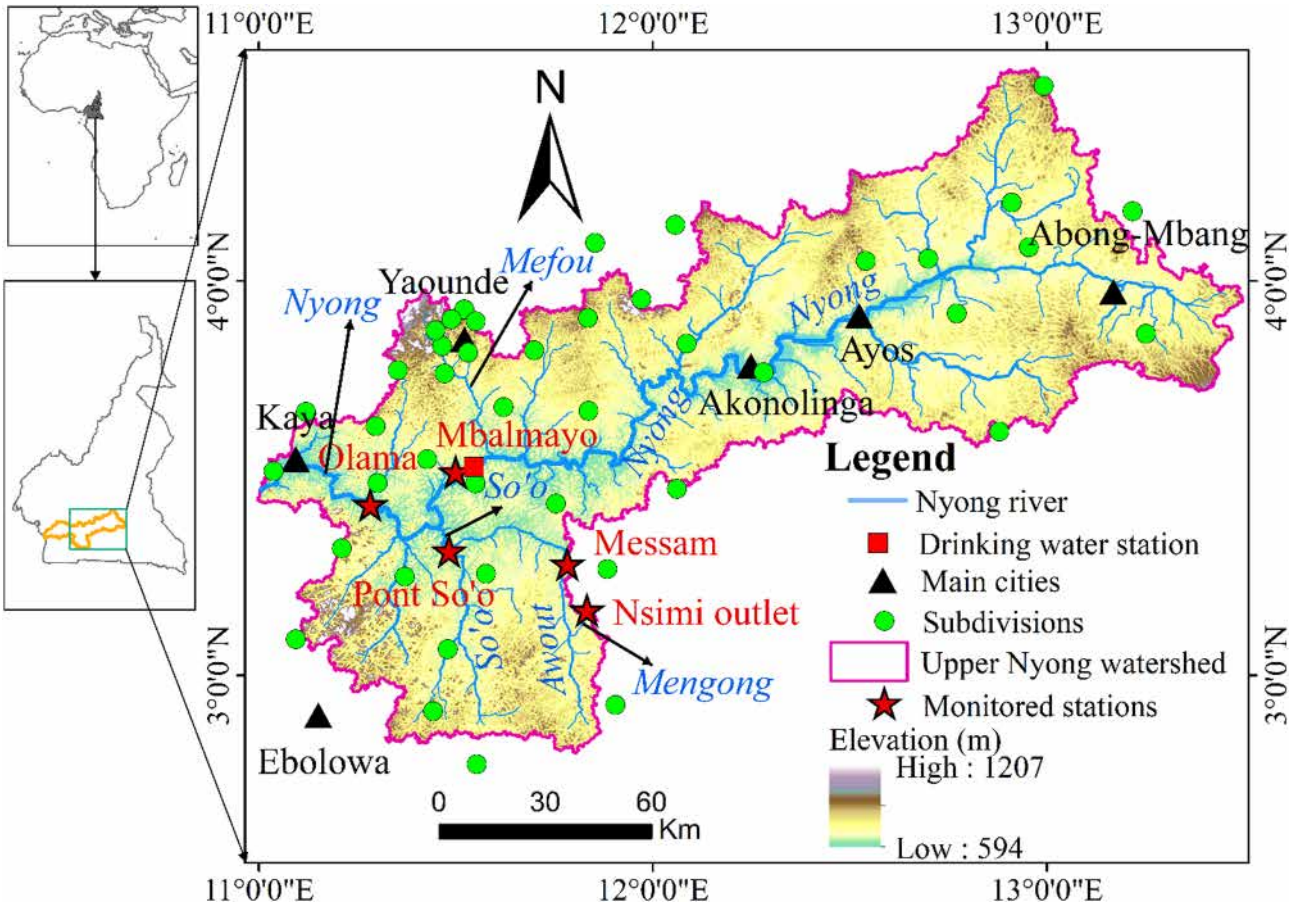

Fig. 1. Main cities, Subdivisions used for population data, orography map and the 5 monitored stations in the upper Nyong basin.

and syenite; (iv) posttectonic meta-dolerite[56–59]. The Ntem unit includes an intrusive series and a banded series as well as a minor quantity of supracrustal rocks[57,60,61].

The UNB is home to the city of Yaounde, one of the country's two main cities, as well as several other important secondary cities. Human activities mainly involve the primary sector, notably agriculture and fishing. However, in the main cities (e.g., Yaounde, Mbalmayo or Akonolinga), there are secondary sector activities such as small carpentry, commerce, crafts, tourism, transport and administrative functions. Despite the inhabitants and related activities, the towns of the UNB do not have waste and wastewater management systems. Thus, waste and wastewater generated in these two towns and others is dumped into the environment without prior treatment. More so, the towns of Yaounde and Mbalmayo are drained by the Mefou tributary, which flows into the Nyong, along the drinking water catchment station (Fig. 1). Hence, the drainage of this waste and wastewater, coupled with the increase in population, is likely to induce changes and deterioration in the quality of the Nyong River water.

In the UNB, to meet their demands, the population uses forest products accompanied with the modification of the landscape. In Cameroon, energy from fuel wood is estimated at 60% of the energy consumed and has been increasing at a rate of 2.5 $\%.y^{-1}$ since 1974-1976[62]. It is estimated that forest provides about 80% of the demands for subsistence to rural communities that fetch fuel wood, hunt animals, farm, gather non-timber forest products and breed animals[62,63]. The UNB is subject to logging for export. According to Gbetnkom[64] forestry sector occupies the first order in export tonnage and third order in foreign earnings. The annual economic value of this sector through veneers saw wood, timber, pulp and parquets can be valued at millions of dollars. It also accounts for 4–10% of the Gross Domestic Product and offer about 40,000 jobs[65–68].

Materials and methods

LUL curacy assessment

The development of the LULC map is based on a methodological approach using remote sensing data and Geographic Information System techniques. This methodological approach includes five steps (Fig. 2): (1) Landsat images collection, (2) pre-processing, (3) processing, (4) classification, and (5) accuracy assessment[69].

Table 1 summarizes the Landsat image collected in this study and presents their corresponding properties. All the Landsat scenes, having a spatial resolution of 30 m, were obtained from the United States Geological Survey (http://earthexplore.usgs.gov). Scenes from Landsat 7 Enhanced Thematic Mapper Plus (ETM+) and Landsat 8 Operational Land Imager (OLI) were used for the years 2005/2010 and 2015/2020 respectively. Three scenes are needed to cover the entire UNB corresponding to paths/rows: 184/057, 185/057 and 185/058.

Southern Cameroon and the Nyong basin are covered by heavy cloud cover throughout the year. Such cloud cover is generally observed in zones located in equatorial and humid tropical climates such as that of the Nyong basin[70]. To illustrate this heaviness, the monthly average cloud cover was calculated from all the scenes captured in the study area between 2000 and 2021 (Fig. 3). During most of the year, cloud cover ranges between 40 and 90%. Cloud cover < 10% is generally tolerated for LULC classification[71–73] but, ideally, cloud cover should be 0%[75–79]. Over the period 2000–2021, out of a total of 458 scenes captured over the UNB, only 17 scenes (3.71%) had cloud cover < 10%. The three scenes covering the entire Nyong basin with cloud cover < 10% could only be obtained for 2015. To compensate this lack for the other years, scenes with cloud cover < 10% and closest in time with the year of interest were chosen to completely cover the study area. For example, scenes 184/057 and 185/057 were chosen in 2004 for the year 2005 (Table 1). Likewise, scene 185/058 was chosen in 2013 for the year 2010, and so on. All the Landsat images collected were proceeded in ArcGIS 10.8 Software.

The collected raw Landsat images were pre-processed which consists of atmospheric/radiometric corrections[38,69,77,78]. These corrections make it possible to remove impurities and eliminate any disturbance affecting spectral signatures of images.

Processing encompasses a set of operations that prepares Landsat images for classification. These operations include: calculation of LULC indices, stacking, mosaicking and subsetting. Three LULC indices were considered in this study, namely: Normalized Difference Water Index (NDWI), Normalized Difference Vegetation Index (NDVI) and Normalized Difference Built-up Index (NDBI). NDWI, NDVI and NDBI respectively highlight the areas cover by open water[79]vegetation[80] and built-up[81]and they were computed as follow

$$NDWI = \frac{\text{Green}-\text{NIR}}{\text{Green}+\text{NIR}} \quad (1)$$

$$NDVI = \frac{\text{NIR}-\text{Red}}{\text{NIR}+\text{Red}} \quad (2)$$

$$NDBI = \frac{\text{SWIR}-\text{NIR}}{\text{SWIR}+\text{NIR}} \quad (3)$$

Where Green is Band 3, NIR (Near InfraRed) is Band 5, Red is Band 4, and SWIR (ShortWave InfraRed) is Band 6, in Landsat 8 OLI imagery. In Landsat 7 ETM+, Green, NIR, Red and SWIR respectively correspond to Band 2, Band 4, Band 3 and Band 5.

Stacking consists of merging the different bands constituting a Landsat scene in order to obtain the composite band. Then, the three composite bands from a given year were mosaicked. From the mosaic obtained, subsetting made it possible to clip out the study area for a classification.

Based on the objective of this study, three classes of objects were defined: the forest (including indifferently pristine and degraded forest, swampy forest), impervious and agricultural surface (bare soil, built-up, agricultural land and roads) and water (river and lake). Using the composite band of the study area, and aided by NDWI, NDVI and NDBI, a supervised image classification technique using the maximum likelihood algorithm was adopted[69,71–73,76,78,85]. This technique assigns each pixel to the object class with the highest likelihood. The

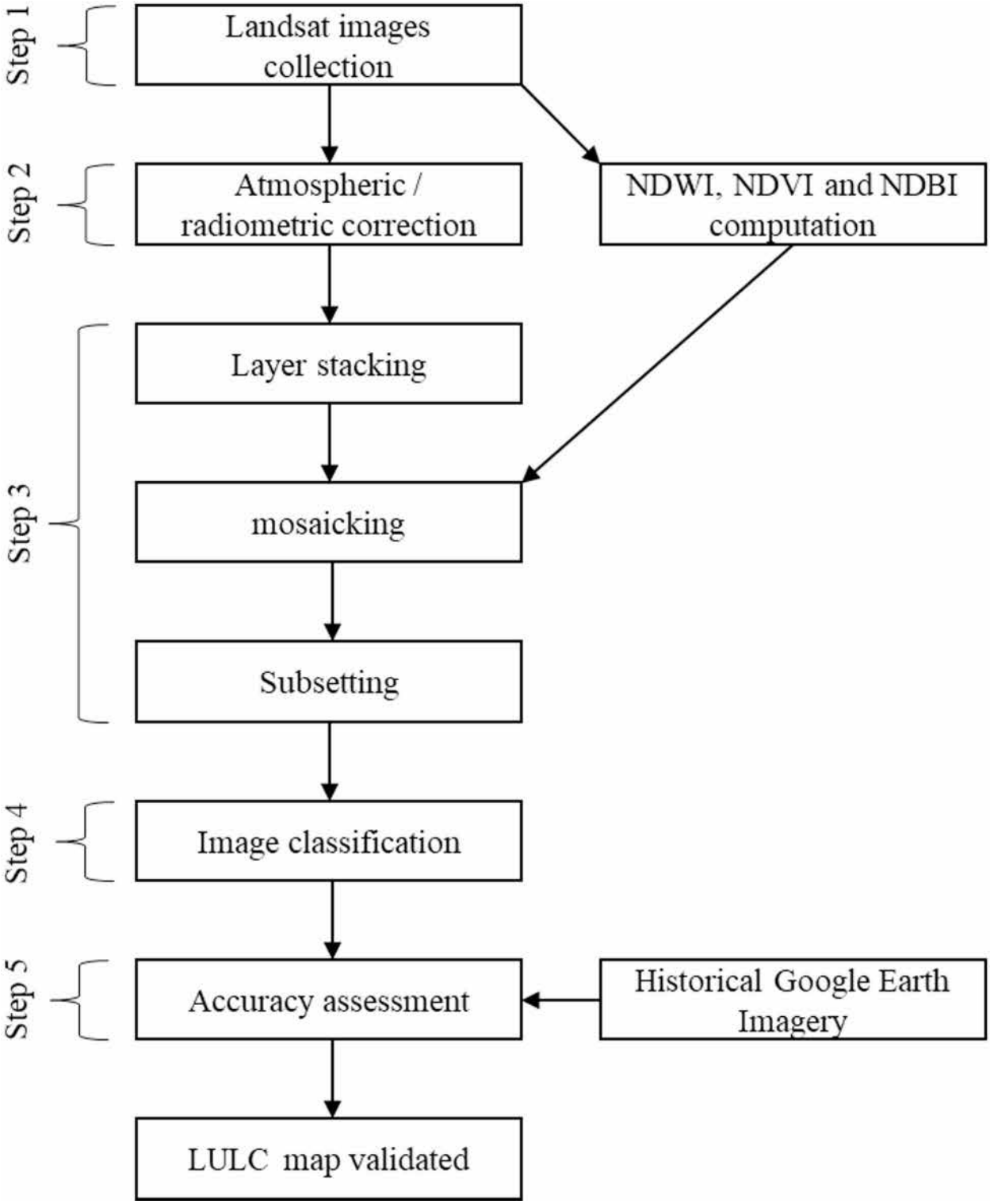

Fig. 2. Flowchart showing the LULC map realization and validation.

number of training points for classification was chosen proportionally to the area of each class in UNB as follows: 1,858,804 sample counts for forest, 26,175 sample counts for impervious and agricultural surface, and 215 samples counts for water (Fig. S1). The LULC map obtained from the classification requires validation by evaluating the accuracy.

Accuracy assessment makes it possible to determine to what degree each pixel is effectively associated with its corresponding object class[83]. For this assessment, stratified random sampling, proportionally distributing the samples between the three object classes, was adopted for the four LULC maps[84]. The accuracy of the LULC

Satellite	Sensor	Path/Row	Resolution (m)	Number of bands	acquisition date	Cloud cover (%)
2005						
Landsat 7	ETM+	184/057	30	7	30/11/2004	2
Landsat 7	ETM+	185/057	30	7	07/02/2004	0
Landsat 7	ETM+	185/058	30	7	08/01/2005	0
2010						
Landsat 7	ETM+	184/057	30	7	17/12/2010	0
Landsat 7	ETM+	185/057	30	7	09/01/2011	0
Landsat 7	ETM+	185/058	30	7	03/03/2013	0.01
2015						
Landsat 8	OLI	184/057	30	8	07/12/2015	0.07
Landsat 8	OLI	185/057	30	8	12/01/2015	0
Landsat 8	OLI	185/058	30	8	13/01/2015	0
2020						
Landsat 8	OLI	184/057	30	8	21/01/2021	0
Landsat 8	OLI	185/057	30	8	26/01/2020	0
Landsat 8	OLI	185/058	30	8	27/01/2020	0.31

Table 1. Properties of Landsat images used in this study.

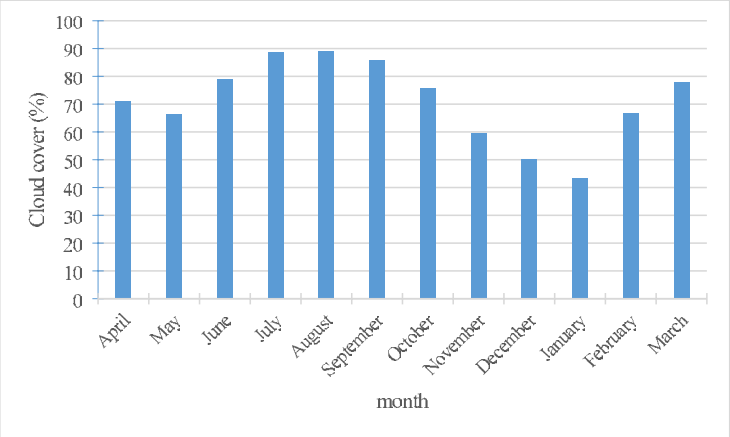

Fig. 3. Average cloud cover per month for the upper Nyong basin, calculated using summary cloud cover statistics calculated from Landsat 7 ETM + and 8 OLI imagery collected between 2000 and 2021.

map samples was determined from the Historical Google Earth Imagery contained in the Google Earth Pro 7 software[74,75]. Comparison of the samples on the LULC maps and the corresponding Historical Images made it possible to generate the confusion matrix which includes users' accuracy, producers' accuracy and kappa coefficient. Based on the kappa coefficient values, which were calculated from users and producers' accuracies, the accuracy of the LULC map is classified as follows: (i) low for kappa < 40%; good for 40% < kappa < 75%, and excellent if kappa > 75%[73].

Discharge, water sampling and analysis

Water chemistry and discharge data used in this study were taken from the hydrochemical and hydrological database produced as part of the Multiscale TROPIcal CatchmentS (M-TROPICS) Critical Zone Observatory (CZO), available in an open-access repository[85–87]. This database was obtained by monitoring 5 stations whose names (Olama, Mbalmayo, Pont So'o, Messam and Nsimi outlet) and characteristics, including those of the corresponding sub-watersheds, are presented in Fig. 1 and Table S1. The sites for stations were chosen so as to have nested basins, that is, from the small experimental Mengong basin at Nsimi outlet to UNB at Olama. This approach makes it possible to monitor the dynamics of hydrological and chemical processes at multiple spatial scales.

Discharge measurement

For discharge measurement, each of the 5 stations studied was equipped with an automatic limnimeter (OTT Hydromet® Thalimede, France; 1-mm resolution) with a 10-min frequency and daily readings on limnimetric scales (staff gages) by local observers[85]. For each of the 4 major stations (Olama, Mbalmayo, Pont So'o and

Messam), the water level obtained from the limnimeter is used to calculate the daily water discharge from a rating curve (relating water level and discharge). The rating curve is obtained from measurements of the average water velocity and the cross-sectional area. A good cross-sectional area stability is indicated by river gauging data available on the watershed and collected by the Research Centre for Water and Climate Change (RCWCC) of Yaounde since 1947. However, the RCWCC is periodically measures discharge to account for riverbed morphology modification that could modify the rating curves. At Nsimi outlet, however, water discharge is computed using a rating curve obtained with a calibrated concrete weir installed at the watershed outlet.

Water sampling and analysis

Water chemistry data resulted from continuous or semi-continuous fortnightly sampling over the period 1994–2021, at Nsimi outlet, and over 1998–2021 at the four other stations (Olama, Mbalmayo, Pont So'o and Messam) in the UNB (Fig. 1). Variables measured in the river include: major dissolved ions (Na^+, K^+, Ca^{2+}, Mg^{2+}, NO_3^-, SO_4^{2-}, F^-, Cl^-, HCO_3^-, Si; µmol. L^{-1}), total Alk (µeq. L^{-1}), DOC (mg. L^{-1}), SPM (mg. L^{-1}), EC (µS. cm^{-1}); pH and WT (°C). Daily discharge was measured at the same stations between 1994 and 2023 for Nsimi outlet, and between 1998 and 2023 for the other four stations.

Each water sample collected was filtered through a cellulose acetate membrane with a pore size of 0.22 µm, then divided into two aliquots which were stored in polypropylene bottles. One of the aliquots was acidified for the measurement of cations (Na^+, K^+, Ca^{2+} and Mg^{2+}), and the other was non-acidified for the determination of anions (NO_3^-, SO_4^{2-}, F^-, Cl^- and HCO_3^-).

Major ion concentration was measured by ion chromatography, spectrophotometer or inductively coupled plasma optical emission spectroscopy (ICP-OES). DOC concentration was measured using total organic carbon (TOC) analyser. SPM concentration was determined by filtration unit with a pore size of 0.7 µm, from a known volume of water. Alk and HCO_3^- were determined by titration using a potentiometric titration. pH, EC and WT, are measured, in situ, using a YSI brand multi-parameter, Professional Plus model. All laboratory operations were carried out at "Laboratoire d'Analyse Géochimique des Eaux" (LAGE; Cameroon) and at the laboratory of "Géosciences Environnement Toulouse" (GET; France). The precision of the analysis is typically 5%, and it is obtained by jointly analyzing certified reference waters[85]. To ensure optimal analytical quality, inter-calibration campaigns are carried out between the LAGE and the GET. They consist of analyzing international standards and replicating analysis on common samples. Further details on discharge measurement, water sampling and analysis methods can be found in Audry et al.[85]. TDS was calculated from EC as proposed by Lloyd and Heathcote[88]

$$TDS = EC \times 0.64 \tag{4}$$

Where TDS is in $mg.L^{-1}$, and EC in $\mu S.cm^{-1}$.

The annual weighted average (C_y) and the monthly weighted average (C_m), were calculated as

$$C_y = \frac{\sum_{i=1}^{n} Q_i C_i}{\sum_{i=1}^{n} Q_i} \tag{5}$$

$$C_m = \frac{\sum_{j=1}^{k} Q_j C_j}{\sum_{j=1}^{k} Q_j} \tag{6}$$

Where C_i represents the value of the physicochemical parameter or the concentration of ions, obtained on a fortnightly scale during the year considered. Q_i is the discharge corresponding to C_i. C_j represents the value of the physicochemical parameter or the concentration of major ions, obtained on a fortnightly scale during the month considered. Q_j is the discharge corresponding to C_j.

Demographic projection

Demographic evolution is one of the main factors influencing LULCC and water quality. However, in sub-Saharan African countries in general, general population censuses do not follow a regular schedule. Thus, studies using demographic trends over time generally make projections based on growth rates[38,39]. Since the existence of the State of Cameroon till its current form, only three general population censuses have been carried out. These censuses are dated 1976[89], 1987[90] and 2005[91]. In order to estimate the evolution profile of the population of the UNB for each of the three census periods, the number of inhabitants of all the Subdivisions located in the basin were pooled together.

To gain an overview of the evolution of population and its impact on LULCC and water quality, a model based on the three censuses was proposed. This model estimates that the population has continued to evolve perfectly as in the past. Before applying the model, the population of the Subdivisions (Fig. 1) of each Division were summed, and then the model was applied for each Division. The UNB extends over a total of 9 Divisions: (1) Dja-et-Lobo (two Subdivisions), (2) Haut-Nyong (seven Subdivisions), (3) Mefou-et-Afamba (six Subdivisions), (4) Mefou-et-Akono (four Subdivisions), (5) Mfoundi (seven Subdivisions), (6) Mvila or Ntem (four Subdivisions), (7) Nyong-et-Mfoumou (five Subdivisions), (8) Nyong-et -Kelle (two Subdivisions), and (9) Nyong-et-So'o (six Subdivisions).

This model estimates that the evolution of the population of each Division is done according to a second-degree equation as follows

$$P(t) = at^2 + bt + c \tag{7}$$

Where P(t) is the population at date t, a, b and c are constants. In practice, c is the population of the Division in 1976, a and b are determined by solving this equation from the known censuses of the three periods 1976, 1987 and 2005. This model has the advantage of integrating all existing census data. On the other hand, projections based on growth rates generally consider data from the first and last censuses, ignoring the intervening years. However the population of the Division of Mefou-et-Afamba decreased between 1976 and 1987, and then increased from 1987 to 2005. Thus, the equation above was inapplicable for this Division and, therefore, the population projection was based on the interannual growth rate calculated from the 1987 and 2005 censuses. The demography of the nine Divisions was subsequently summed to obtain that of the UNB in December of the years 2005, 2010, 2015 and 2020.

Atmospheric temperature and rainfall data

Atmospheric temperature and rainfall data used here were obtained from Climatic Research Unit gridded Time Series 4.07 (CRU TS 4.07), in Google Earth Pro 7 software. CRU TS is a widely used climate dataset on a 0.5° latitude by 0.5° longitude grid over all land domains of the world except Antarctica[92]. It is derived by the interpolation of monthly climate anomalies from extensive networks of weather station observations. Conveniently, the CRU TS 4.07 database was downloaded from https://crudata.uea.ac.uk/cru/data/hrg/cru_ts_4.07/ge/. Subsequently, this database was opened in Google Earth Pro 7, where the atmospheric temperature and rainfall data for the area of each station were downloaded. On the other hand, daily rainfall data exist within the framework of M-TROPICS and are available at[93]: https://doi.org/10.6096/BVET.CMR.METEO. Despite having many gaps, this dataset was aggregated to monthly data, when possible, and used to validate the corresponding satellite data at the Nsimi outlet station.

Solute fluxes to the sea were calculated on an annual basis (Eq. 8) and on a monthly basis (Eq. 9) as follows[94]

$$F_y = \frac{C_y \times V_y}{S} \quad (8)$$

$$F_m = \frac{C_m \times V_m}{S} \quad (9)$$

Where F_y represents the annual flux in $t.km^{-2}.y^{-1}$ and F_m the monthly flux in $mg.km^{-2}.m^{-1}$. C_y and C_m respectively represent the annual discharge-weighted average and the monthly discharge-weighted average, converted to $\mu g.L^{-1}$, for TDS, Na^+, K^+, Ca^{2+}, Mg^{2+}, NO_3^-, SO_4^{2-}, F^-, Cl^-, HCO_3^-, SiO_2, DOC and SPM. V_y and V_m respectively correspond to the annual and monthly discharge, in $km^{-3}.y^{-1}$ and $km^{-3}.m^{-1}$, calculated by making the arithmetic sum of the daily discharge. S represents the surface area of the sub-watershed corresponding to each of the five stations monitored (Table S1).

The long-term trend in rainfall and solute fluxes were performed through the RStudio software version 4.4.1 (2024-06-14 Universal C Runtime) using Pettitt test and Modified Mann-Kendall trend test. For this, discharge, precipitation and atmospheric temperature (AT) were first subjected to the Pettitt's test in order to detect a possible change point in Q, precipitation and AT trends[95]. The Pettitt test provides two parameters: the p-value and a change time k. When the p-value is <0.01, the change in trend is considered significant, and time k is considered the change point. On the other hand, when the p-value >0.01, there is no change in the time series, here rainfall or AT. In the absence of a change point, Q was associated with solute concentrations, and rainfall with solute fluxes, to perform the Modified Mann-Kendall Test[96–99]. The Modified Mann Kendall Test used here is that of Yue and Wang[99] which consists of determining the existence or not of a trend in a time series, addressing the issue of the possible existence of serial autocorrelation in trend analysis. The existence or not of a trend is determined from the calculation of three parameters: tau (τ), the new p-value (p) and slope. τ indicates the direction of the trend, while p determines whether the trend is significant or not. When $\tau > 0$, the trend is positive and vice versa. The trend is considered significant when $p < 0.01$. Finally, the slope quantifies the trend.

Graphs and descriptive statistics were produced in Excel 2016 Pro Plus software. Analysis of variance (ANOVA) for differences of spatial concentrations, with significance at $p < 0.01$, was carried out in Statistical Package for Social Sciences (SPSS 18.0 for Windows, SPSS Inc., USA).

Results

Accuracy assessment

Table 2 presents confusion matrix with results of users' accuracy, producers' accuracy, overall accuracy and kappa coefficient of the LULC classes for periods 2005, 2010, 2015 and 2020. For the four periods, the users' accuracy values varied from 70 to 100%, while those of producers' accuracy ranged from 95.7 to 100%. The overall accuracy is 97.3% for the year 2005, 96.4% for the year 2010 and 100% for the years 2015 and 2020. The kappa coefficient values are distributed as follows: 90.7% for the year 2005, 88.4% for the year 2010, and 100% for the years 2015 and 2020. Based on these values, the classification carried out in this study is excellent (kappa > 75%).

Areal composition and LULCC

The results on the LULC composition and changes are presented in Fig. 4a-d; Tables 3 and 4. Over the period examined, forest remained the dominant LULC class with an area varying from 17,845 km^2 (92.77%) in 2005 to 16,638 km^2 (86.49%) in 2020. The impervious and agricultural surface vary from 1376 km^2 (7.15%) to 2587 km^2 (13.45%) for the four periods. The area of water vary from 15 km^2 (0.08%) to 11 km^2 (0.06%).

First, the area covered by water is negligible compared to the areas covered by forest and impervious and agricultural surface. Because of this negligible nature, this section will not put much emphasis on the water result,

Class Value	Forest	impervious and agricultural surface	Water	Total	Users Accuracy	Kappa
2005						
Forest	91	0	0	91	1	0
impervious and agricultural surface	3	7	0	10	70%	0
Water	0	0	10	10	1	0
Total	94	7	10	111	0	0
Producers Accuracy	96.8%	1	1	0	97.3%	0
Kappa	0	0	0	0	0	90.7%
2010						
Forest	88	0	0	88	1	0
impervious and agricultural surface	3	9	0	12	75%	0
Water	1	0	9	10	90%	0
Total	92	9	9	110	0	0
Producers Accuracy	95.7%	100%	100%	0	96.4%	0
Kappa	0	0	0	0	0	88.4%
2015						
Forest	89	0	0	89	100%	0
impervious and agricultural surface	0	11	0	11	100%	0
Water	0	0	10	10	100%	0
Total	89	11	10	110	0	0
Producers Accuracy	100%	100%	100%	0	100%	0
Kappa	0	0	0	0	0	100
2020						
Forest	86	0	0	86	100%	0
impervious and agricultural surface	0	13	0	13	100%	0
Water	0	0	10	10	100%	0
Total	86	13	10	109	0	0
Producers Accuracy	100%	100%	100%	0	100%	0
Kappa	0	0	0	0	0	100

Table 2. Confusion matrix showing accuracy assessment of LULC maps for the years 2005, 2010, 2015 and 2020.

which is probably within the error margin of the data processing or calculations. In general, between 2000 and 2020, there is a progressive decrease in the forest and water areas, and a progressive increase of impervious and agricultural surface. Based on their level of decline, the three periods are arranged in descending order as such: 2005–2010 > 2015–2020 > 2010–2015 with absolute values of LULCC of 547 km^2 (3.07%), 444.7 km^2 (2.60%) and 215.3 km^2 (1.24%), respectively. The impervious and agricultural surface was 1,376 km^2 in 2005 (7.15%), and it gradually increased to 1,924 km^2 (10.00%), 2,140 km^2 (11.13%) and 2,587 km^2 (13.45%) in 2010, 2015, and 2020, respectively. In the same order of decrease in the forest area, the impervious and agricultural surface increases as such: 2005–2010 > 2015–2020 > 2010–2015 with values of 548 km^2 (39.83%), 447 km^2 (20.89%), and 216 km^2 (11.23%), respectively. However, during the same period, a net increase of 1,211 km^2 (88.01%) of impervious and agricultural surface is observed. Spatially, deforestation and expansion of impervious and agricultural surface are mainly taking place in and around the city of Yaounde (Mfoundi). The relative evolution of the forest area and impervious and agricultural surface between the 3 periods above can be explained by factors that occurred on a countrywide scale. Indeed, from 1992 to 2003, agricultural areas remained stable at 91,600 km^2 (19.4% of Cameroonian territory)[100–102]. From 2004, agricultural area began to grow rapidly, which continued until 2010 when it reached 97,500 km^2 (20.6% of Cameroonian territory). Thus, over a period of 8 years, agricultural areas increased by 5,600 km^2 across the country. This increase is the first factor that can explain the deforestation and relative increase in impervious and agricultural surface in Nyong basin. Since 2011, the amount of agricultural land has been generally stable in Cameroon, and it cannot be an important factor in explaining the changes that occurred after that year. The second factor is linked to the crisis that has been shaking the North-West and South-West Regions of Cameroon since 2016. This crisis has led to an internal displacement of masses of people mainly to the two main cities of the country, Yaounde and Douala, and to a lesser extent to other secondary cities in the country. These movements have generated, in both cities, strong demands related to housing, food, work, etc., hence the relatively increase in impervious and agricultural surface between 2015 and 2020. The loss of forest/water area and growth of impervious and agricultural surface has also been observed in more localized studies in the UNB[32,34,36,37]in southern Cameroon[88] and in humid tropical Sub-Saharan Africa[72–73,75–76,81].

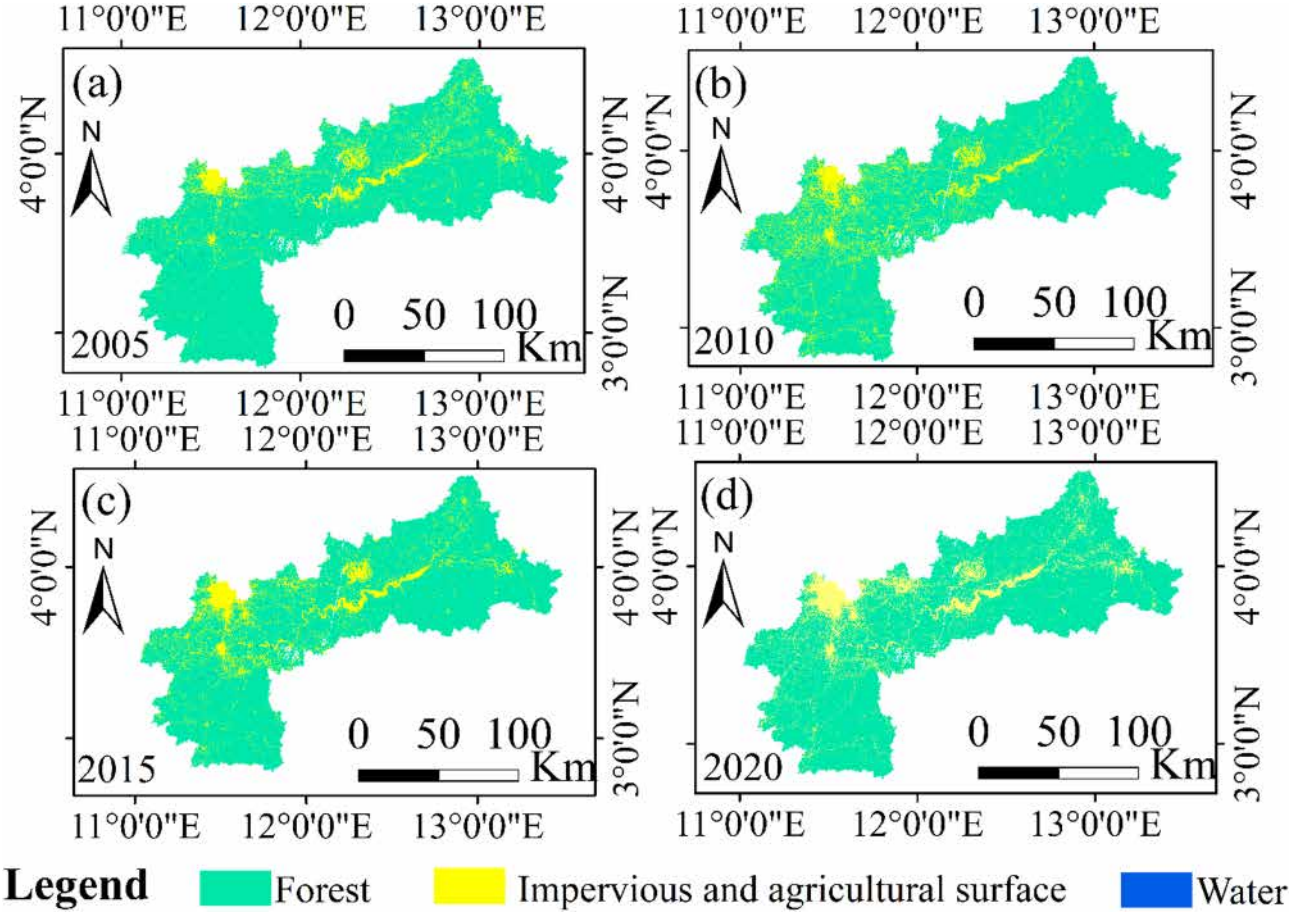

Fig. 4. LULC classification maps of the upper Nyong basin for 2005 (a), 2010 (b), 2015 (c) and 2020 (d).

LULC	2005		2010		2015		2020	
	Area (km^2)	Area (%)	Area (km^2)	Area (%)	Area (km^2)	Area (%)	Area (km^2)	Area (%)
Forest	17,845	92.77	17,298	89.93	17,082.7	88.81	16,638	86.49
impervious and agricultural surface	1,376	7.15	1,924	10.00	2,140	11.13	2,587	13.45
Water	15.00	0.08	14.00	0.07	13.30	0.07	11.00	0.06
Total	19,236	100	19,236	100	19,236	100	19,236	100

Table 3. LULC composition of the upper Nyong basin in 2005, 2010, 2015 and 2020.

LULC	2005–2010		2010–2015		2015–2020		2005–2020	
	Area (km^2)	Area (%)	Area (km^2)	Area (%)	Area (km^2)	Area (%)	Area (km^2)	Area (%)
Forest	−547	−3.07	−215.3	−1.24	−444.7	−2.60	−1,207	−6.76
impervious and agricultural surface	548	39.83	216	11.23	447	20.89	1,211	88.01
Water	−1.0	−6.67	−0.7	−5.00	−2.3	−17.29	−4.0	−26.67

Table 4. LULCC of the upper Nyong basin for the periods 2005–2010, 2010–2015, 2015–2020 and 2005–2020.

LULCC rate

Table 5 shows LULCC rates for the three defined periods. The forest and water areas depicted continuous decrease during all the study period (2000–2020) with net rates of change of −80.5 $km^2.y^{-1}$ (−0.45 $\%.y^{-1}$) and −0.3 $km^2.y^{-1}$ (−1.78 $\%.y^{-1}$) respectively. For the forest, the decreasing rate with respect to the three periods ranges in descending order: 2005–2010 > 2015–2020 > 2010–2015 with absolute values of 109.4 $km^2.y^{-1}$ (0.61 $\%.y^{-1}$), 88.9 $km^2.y^{-1}$ (0.52 $\%.y^{-1}$) and 43.1 $km^2.y^{-1}$ (0.25 $\%.y^{-1}$) respectively. Unlike the forest, the impervious and

LULC	2005–2010		2010–2015		2015–2020		2005–2020	
	Area ($km^2.y^{-1}$)	Area ($\%.y^{-1}$)	Area ($km^2.y^{-1}$)	Area ($\%.y^{-1}$)	Area ($km^2.y^{-1}$)	Area $\%.y^{-1}$)	Area ($km^2.y^{-1}$)	Area $\%.y^{-1}$)
Forest	−109.4	−0.61	−43.1	−0.25	−88.9	−0.52	−80.5	−0.45
impervious and agricultural surface	110.6	7.97	43.2	2.25	89.4	4.18	80.8	5.87
Water	−0.2	−1.33	−0.1	−1.00	−0.5	−3.46	−0.3	−1.78

Table 5. LULCC rate of the upper Nyong basin for the periods 2005–2010, 2010–2015, 2015–2020 and 2005–2020.

	Rate of change ($\%.y^{-1}$)		
	Forest	impervious and agricultural surface	
Upper Nyong basin (Cameroon)	−0.5	5.9	This study
Congo Basin	−0.1	-	
Cameroon[103–105]	−0.3	-	
Upper Nyong basin (Cameroon)[34]	−0.2	8.3	
Mbalmayo (Nyong basin, Cameroon)[37]	−0.6	2.7	
Centre Region of Cameroon[108]	−1.7	-	
Mungo basin (Cameroon)[106]	−0.6	3.8	
Ankobra basin (Ghana)[75]	−0.54	15	
Hangar basin (Abay basin, Ethiopia)[76]	−1.1	0.1	
Mpologoma basin (eastern Uganda)[72]	−1	0.7	
Budongo-Bugoma landscape (Uganda)[73]	−0.6	0.2	
Atwima Nwabiagya North (Ghana)[81]	−1.9	9.2	

Table 6. Rates of change of LULC layers of the upper Nyong basin compared to congo basin, Cameroon area, other zones and basins in Southern Cameroon and humid tropical sub-Saharan africa.

LULC classes	Forest	impervious and agricultural surface	Water	Total in 2005
Forest	16,190	1,655	0	17,845
impervious and agricultural surface	447	929	0	1,376
Water	1.2	2.8	11	15
Total in 2020	16,638	2,587	11	19,236

Table 7. Transition matrix of LULC conversion, in km^2, in the upper Nyong basin between 2005 and 2020.

agricultural surface increases over the entire study period with a net increase rate of 80.8 $km^2.y^{-1}$ (5.87 $\%.y^{-1}$). In the same order like forest, impervious and agricultural surface increasing rate ranges such that 2005–2010 > 2015–2020 > 2010–2015 with rate of change values of 110.6 $km^2.y^{-1}$ (7.97 $\%.y^{-1}$), 89.4 $km^2.y^{-1}$ (4.18 $\%.y^{-1}$) and 43.2 $km^2.y^{-1}$ (2.25 $\%.y^{-1}$) respectively.

Table 6 presents a comparison between the LULCC rates of the UNB, Congo Basin, Cameroon area, and other zones and basins in southern Cameroon and humid tropical sub-Saharan Africa. In the Congo Basin, the interannual deforestation rate was 0.1% between 2000 and 2010[107]. In the UNB, deforestation rate is three times higher than that in the Congo Basin. The deforestation rate obtained in this study (–0.5 $\%.y^{-1}$) is also higher than that obtained by Ebodé et al.[34]but lower than that obtained by Mingang et al.[37]in the UNB. In addition, the deforestation rate in the UNB is lower than that of the Centre Region of Cameroon, Mungo and other basins and zones in humid tropical sub-Saharan Africa. The rate of increase in impervious and agricultural surface (5.9 $\%.y^{-1}$) is lower than that observed by Ebodé et al.[34] in the UNB (8.3 $\%.y^{-1}$), as well as those in the Ankobra basin and the Atwima Nwabiagya North zone, in Ghana[74]. On the other hand, the rate of increase in impervious and agricultural surface in the UNB is lower than those observed in Mbalmayo, Mungo and other zones and basins of humid tropical sub-Saharan Africa. The high rate of deforestation in UNB, compared to Cameroon and the entire Congo Basin, can be associated with the high relative population density.

Transition matrix

Table 7 shows the transition matrix and Fig. 5 presents the conversion of LULC classes between 2005 and 2020. In the study period, conversion of forest to impervious and agricultural surface is clearly visible while the other conversions appear with difficulty or do not appear at all (Fig. 5). Of the 17,845 km^2 forest area

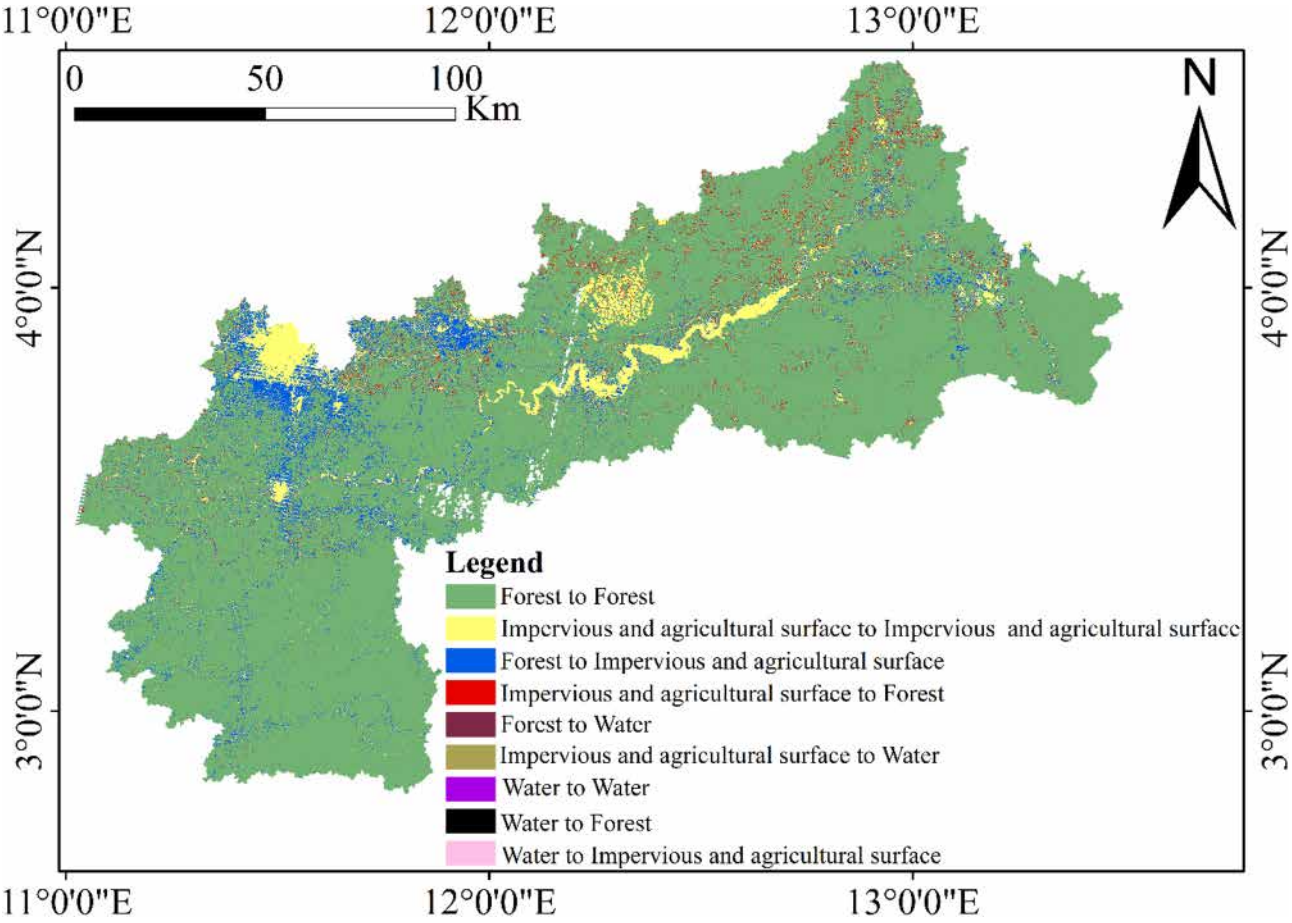

Fig. 5. LULC conversion in the upper Nyong basin between 2005 and 2020.

observed in 2005, 16,189.8 km^2 of forest area are preserved, and 1,655 km^2 are transformed into impervious and agricultural surface. In addition, 447 km^2 of impervious and agricultural surface and 1.2 km^2 of water area are transformed into forest. The impervious and agricultural surface increases from 1,376 km^2 to 2,587 km^2 between 2005 and 2020. In 2020, 929 km^2 of impervious and agricultural surface are preserved, and the surplus results from the conversion of the forest surface and very little of the water area with 2.8 km^2. With a value of 15 km^2 in 2005, 11 km^2 of water area is preserved in 2020, the surplus having been converted into forest (1.2 km^2) and impervious and agricultural surface (2.8 km^2).

Population growth

Projection model parameters, population recorded in historical censuses (1976, 1987 and 2005), projected population (2005, 2010, 2015 and 2020) and population density, in the UNB, are presented in Table 8. Historical censuses recorded 750,346 inhabitants (39 $inhabitants.km^{-2}$) in April 1976, 1,232,447 inhabitants (64 $inhabitants.km^{-2}$) in April 1987 and 2,559,390 inhabitants (133 $inhabitants.km^{-2}$) in November 2005. Based on these historical censuses[89–91]projected populations in December of the years 2005, 2010, 2015 and 2020 are respectively 2,596,668 inhabitants (135 $inhabitants.km^{-2}$), 3,059,995 inhabitants (159 $inhabitants.km^{-2}$), 3,567,045 inhabitants (185 $inhabitants.km^{-2}$) and 4,117,819 inhabitants (214 $inhabitants.km^{-2}$). Based on the 1976 and 2005 censuses, the interannual population growth rate in Nyong is 8.1 $\%.y^{-1}$. This rate is almost double that of Cameroon over the same period (4.3 $\%.y^{-1}$), and is lower than those of the country's two main cities, Yaounde (Mfoundi, 16.9 $\%.y^{-1}$) and Douala (12.2% $\%.y^{-1}$). According to projections, in 2020, the city of Yaounde alone contains 80.1% of the entire population of UNB. The city of Yaounde can therefore be considered as the main factor responsible for the higher growth rate of the UNB compared to the national rate. The city hosts the main institutions of the country with the populations tasked to carry out administrative functions. These institutions and the personnels indirectly create the demand and possibilities for activities such as real estate, agriculture, education, trade, etc. All this explains the deforestation and expansion of impervious and agricultural surface in and around Yaounde, as mentioned above.

Characteristics of water chemistry

Major ions and physicochemical parameters characteristics

The hydrochemical characteristics of the Nyong basin during the sampling period are presented in Table 9. Except Mg^{2+} and NO_3^-, all physicochemical parameters and major ions generally show significant spatial

Divisions	Model parameters			Recorded population			Projected population			
	a	b	c	1976*	1987*	2005**	2005***	2010***	2015***	2020***
Dja-et-Lobo	−9.77	1,602.20	74,248	74,248	90,690	113,096	113,182	118,050	122,430	126,321
Haut-Nyong	−20.82	2,032.99	73,350	73,350	93,194	115,274	115,341	118,810	121,238	122,625
Mefou-et-Afamba	-	-	-	57,348	53,936	74,179	74,738	78,244	81,749	85,255
Mefou-et-Akono	−19.79	1,875.26	50,284	50,284	55,446	59,017	88,498	91,508	93,528	94,559
Mfoundi	943.65	25,109.11	313,206	313,206	703,588	1,881,876	1,888,628	2,317,715	2,793,984	3,317,436
Mvila (Ntem)	−6.37	1,828.40	9,397	9,397	28,739	57,915	58,036	65,130	71,906	78,363
Nyong-et-Mfoumou	−18.19	1,607.74	72,865	72,865	88,349	104,507	104,552	106,739	108,017	108,385
Nyong-et-Kelle	25.55	−224.29	21,843	21,843	22,467	37,566	37,674	44,770	53,144	62,795
Nyong-et-So'o	−19.79	1,875.26	77,805	77,805	96,038	115,960	116,019	119,029	121,049	122,080
Total	-	-	-	**750,346**	**1,232,447**	**2,559,390**	**2,596,668**	**3,059,995**	**3,567,045**	**4,117,819**
Density ($\mathrm{inha.km^{-2}}$)	-	-	-	**39**	**64**	**133**	**135**	**159**	**185**	**214**

Table 8. Population projection model parameters, census data from 1976, 1987 and 2005, and projected populations for 2005, 2010, 2015 and 2020 per division in the upper Nyong basin. *Recorded in April of the corresponding year[89,90]. **Recorded in November of the corresponding year[91]. ***Projected in December of the corresponding year (this study).

differences ($p < 0.01$, ANOVA) in mean values and concentrations for the 5 stations. WT varies between 13.7 and 33.8 °C with arithmetic average of 24.8 °C. The mean temperature value is very close to the average ambient temperature of the southern plateau of Cameroon (25 °C)[46,47]. Alabaster and Lloyd[103] reported that temperature of natural inland waters in the tropics generally varied from 25 to 35 °C. In this study, 54.60% of the samples showed temperature values below 25 °C.

pH values range between 4.4 and 8.5 with arithmetic average of 5.8, i.e. slightly acidic. Based on the weighted average value, the stations range as follows: Olama > Mbalmayo > Pont So'o > Nsimi outlet > Messam, showing that the Nyong River is less acidic than its tributaries. Notably, Awout is the most acidic river. Seven samples however showed a pH above 7, and may constitute a fingerprint of anthropogenic effects on the quality of the river.

EC varies between 11.9 and 96.5 $\mu\,\mathrm{S.cm^{-1}}$, with arithmetic mean of 24.4 $\mu\,\mathrm{S.cm^{-1}}$. TDS varies between 7.6 and 61.8 $\mathrm{mg.L^{-1}}$, with arithmetic mean of 15.6 $\mathrm{mg.L^{-1}}$. The EC and TDS values reflect the poor mineralization of these streams draining lateritic soils. The Nyong River is more mineralised than its tributaries. The stream of the smallest basin, the Mengong, is the least mineralised.

Alk varies between 9.9 and 480 $\mu\,\mathrm{eq.L^{-1}}$ with arithmetic mean of 96.2 $\mu\,\mathrm{eq.L^{-1}}$. Based on the weighted average value, the stations range in the following order: Mbalmayo > Olama > Nsimi outlet > Pont So'o > Messam, suggesting that Nyong is more alkaline than its tributaries and Awout is the least alkaline.

DOC ranges between 6.44 and 73.5 $\mathrm{mg.L^{-1}}$ with arithmetic mean of 20. Based on the average DOC values, the stations studied are classified as follows: Messam > Nsimi outlet > Pont So'o > Mbalmayo > Olama, suggesting a decrease in DOC values from the tributaries towards the main course of the Nyong River.

SPM ranges between 0 and 108 $\mathrm{mg.L^{-1}}$, with arithmetic mean of 16.7 $\mathrm{mg.L^{-1}}$. Based on the weighted average, the stations are ranked as follows: Pont So'o > Olama > Mbalmayo > Messam > Nsimi outlet.

For each station, the average concentration of SiO_2 is always higher than the average concentrations of the corresponding cations and anions. Apart from the Messam station, the major cations rank as follows, for all other stations, based on the weighted average: $Na^+ > Ca^{2+} > Mg^{2+} > K^+$. For the Messam station, the major cations rank as follows based on the weighted average: $Ca^{2+} > Na^+ > Mg^{2+} > K^+$. The major anions are classified as follows, for all stations, based on the weighted mean: $HCO_3^- >> Cl^- >> SO_4^{2-} > NO_3^- > F^-$. Generally, the weighted averages are higher at the stations of the main Nyong channel (Olama and Mbalmayo) compared to those of the tributaries (Pont So'o, Messam and Nsimi outlet). In addition, average concentrations are higher in Mbalmayo compared to Olama.

All physicochemical parameters and major ions are higher in the Mefou compared to the Nyong rivers. Specifically, except WT, pH and SiO_2, which are slightly higher, all other parameters are 2.8 to 59.5 times higher in the Mefou compared to the Nyong rivers. This suggests that the Mefou is the origin of the enrichment of the Nyong (Olama and Mbalmayo) compared to its tributaries. The high densification and growth of the population in Yaounde, as well as the corresponding deforestation and development of impervious and agricultural surface, induce a production of waste and wastewater. Due to the inadequacy of the system for their management, waste and wastewater are first drained by the Mefou into the Nyong at Mbalmayo, before joining Olama. In addition, in the context of the other three stations, the densification and growth of the population remain moderate. Thus, deforestation and the increase of impervious and agricultural surface remain reduced, and the waste and wastewater produced is less important. Furthermore, to clearly understand the link between population growth, LULCC and the geochemical functioning of the Nyong rivers, it would be important to consider the evolution of solute specific fluxes over the studied period.

All studied rivers						
	arithmetic			Min	Max	Med
	n	Mean	sd			
WT	1,568	24.8	1.7	13.7	33.8	24.8
pH	1,605	5.8	0.5	4.4	8.5	5.8
EC	1,635	24.4	9.1	11.9	96.5	21.8
TDS	1,635	15.6	5.8	7.6	61.8	14
Na^+	1,827	62.7	30.8	10	403.0	55.4
K^+	1,827	23.3	20.8	0	425.1	19.8
Mg^{2+}	1,812	29.4	8.9	0	176.3	27.9
Ca^{2+}	1,828	45.9	17.4	8.8	238.3	42.5
F^-	879	1.7	2.0	0	22.3	1.4
Cl^-	1,766	21.3	19.7	0	199.0	15.9
NO_3^-	1,764	3.1	7.0	0	97.7	0
SO_4^{2-}	1,757	5.6	10.7	0	190.1	2.5
Alk	1,214	96.2	61.8	9.9	480	81
HCO_3^-	1,096	97.6	63.7	9.9	479.8	80.8
Si	1,334	140.1	28.8	0	307.6	140.4
DOC	1,279	20.0	7.7	6.4	73.5	18.3
SPM	1,532	16.7	9.5	0	108.0	14.9

The Nyong, its tributaries and Mefou River						
	Weighted mean					Arithmetic mean
	Olama	Mbalmayo	Pont So'o	Messam	Nsimi outlet	Mefou[110]
WT	25.2	25.4	23.8	23.4	24.1	26.4
pH	5.9	5.9	5.7	5.2	5.5	6.4
EC	23.8	25.3	19.4	21.2	17.8	220.5
TDS	15.2	16.2	12.4	13.5	11.4	102.2
Na^+	53.8	57.3	48.7	40.8	52.6	760.9
K^+	24.0	26.2	25.4	23.3	12.8	163.7
Mg^{2+}	28.3	29.6	25.9	25.3	23.9	104.9
Ca^{2+}	44.8	47.5	37.9	45.0	34.1	322.9
F^-	1.9	1.9	1.5	1.5	1.4	5.3
Cl^-	24.5	26.6	13.3	12.4	9.9	456.3
NO_3^-	2.6	2.5	2.7	1.7	1.0	61.3
SO_4^{2-}	4.5	4.2	4.1	3.1	1.5	40.6
Alk	101.1	106.3	61.4	47.4	72.1	-
HCO_3^-	103.6	106.4	62.0	48.9	71.7	1175.4
Si	126.2	114.1	149.7	141.1	136.0	204.7
DOC	17.9	18.0	19.8	27.6	20.0	-
SPM	16.7	15.0	20.1	15.0	12.7	-

Table 9. Long-term average hydrochemical characteristics of the upper Nyong basin rivers compared to Mefou river. WT in °C, EC in $\mu S.cm^{-1}$, DOC and SPM in $mg.L^{-1}$, major ions (Na^+, K^+, Mg^{2+}, Ca^{2+}, F^-, Cl^-, NO_3^-, SO_4^{2-} et HCO_3^-) and SiO_2 in $\mu mol.L^{-1}$, and Alk in $\mu eq.L^{-1}$.

Long-term variation in Climatic parameters, discharge, physicochemical parameters and major ions

The long-term fortnightly variation, of discharge (Q), atmospheric temperature (AT), physicochemical parameters and major ions concentrations, with respect to the seasons, for the 5 stations is presented in Figs. 6 and 7 and S3-S5. The result of the Modified Mann-Kendall test applied to daily discharge, monthly AT, fortnightly physicochemical parameters and major ions, and interseasonal parameters, is presented in Table S2.

Exploring discharge and atmospheric temperature trend change point The Pettitt's test applied to the long-term variation of discharge, on daily, interseasonal and interannual base, gave p-values > 0.01 for the 5 stations.

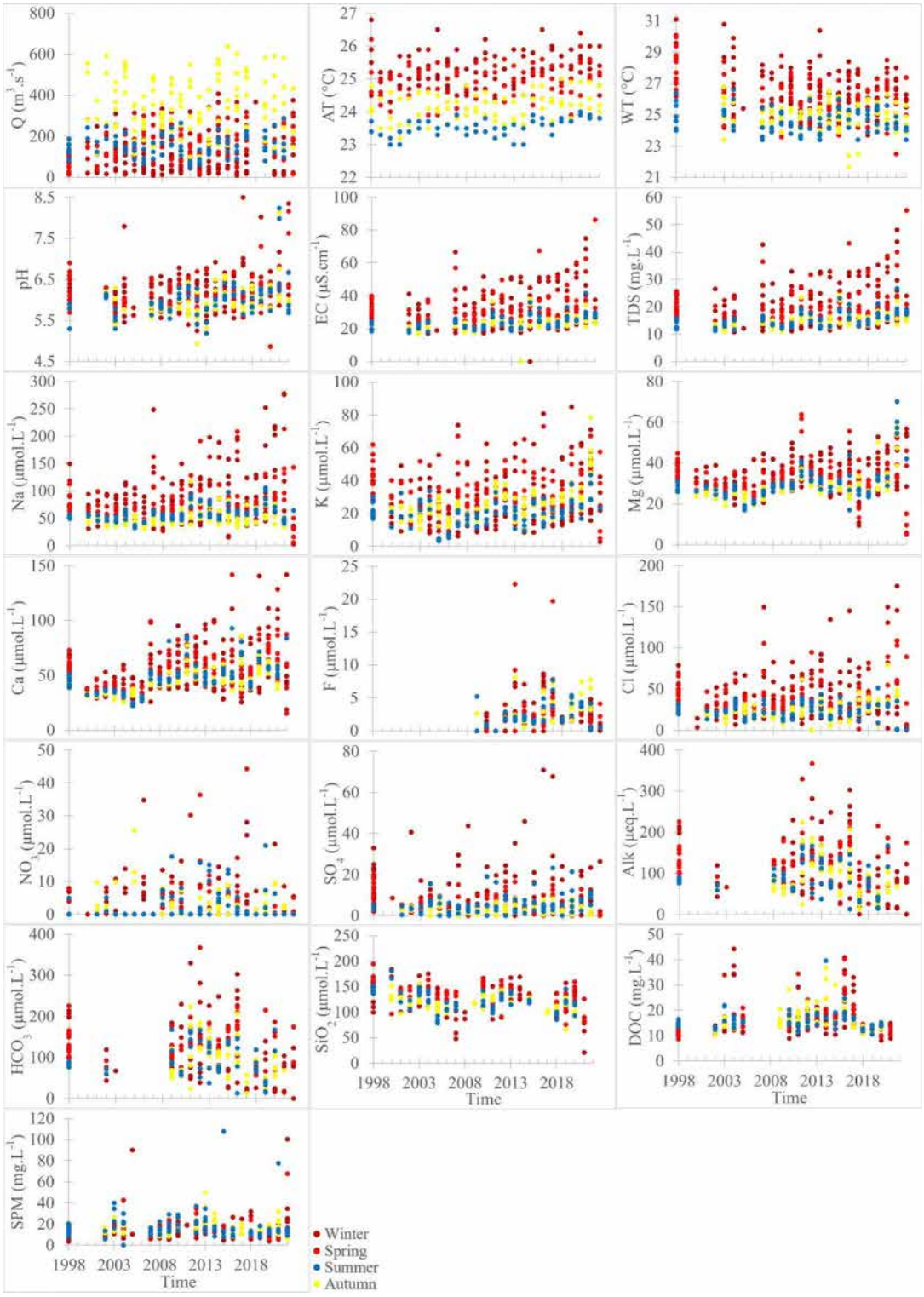

Fig. 6. Long-term fortnightly variation, depending on the seasons, for: discharge (Q), atmospheric temperature (AT), WT, pH, EC, concentrations of TDS, concentrations of major cations (Na^+, K^+, Mg^{2+}, Ca^{2+}), concentrations of major anions (F^-, Cl^-, NO_3^-, SO_4^{2-}, HCO_3^-), concentrations of SiO_2, concentrations of DOC, and concentrations of SPM at Olama station, over the period 1998–2022.

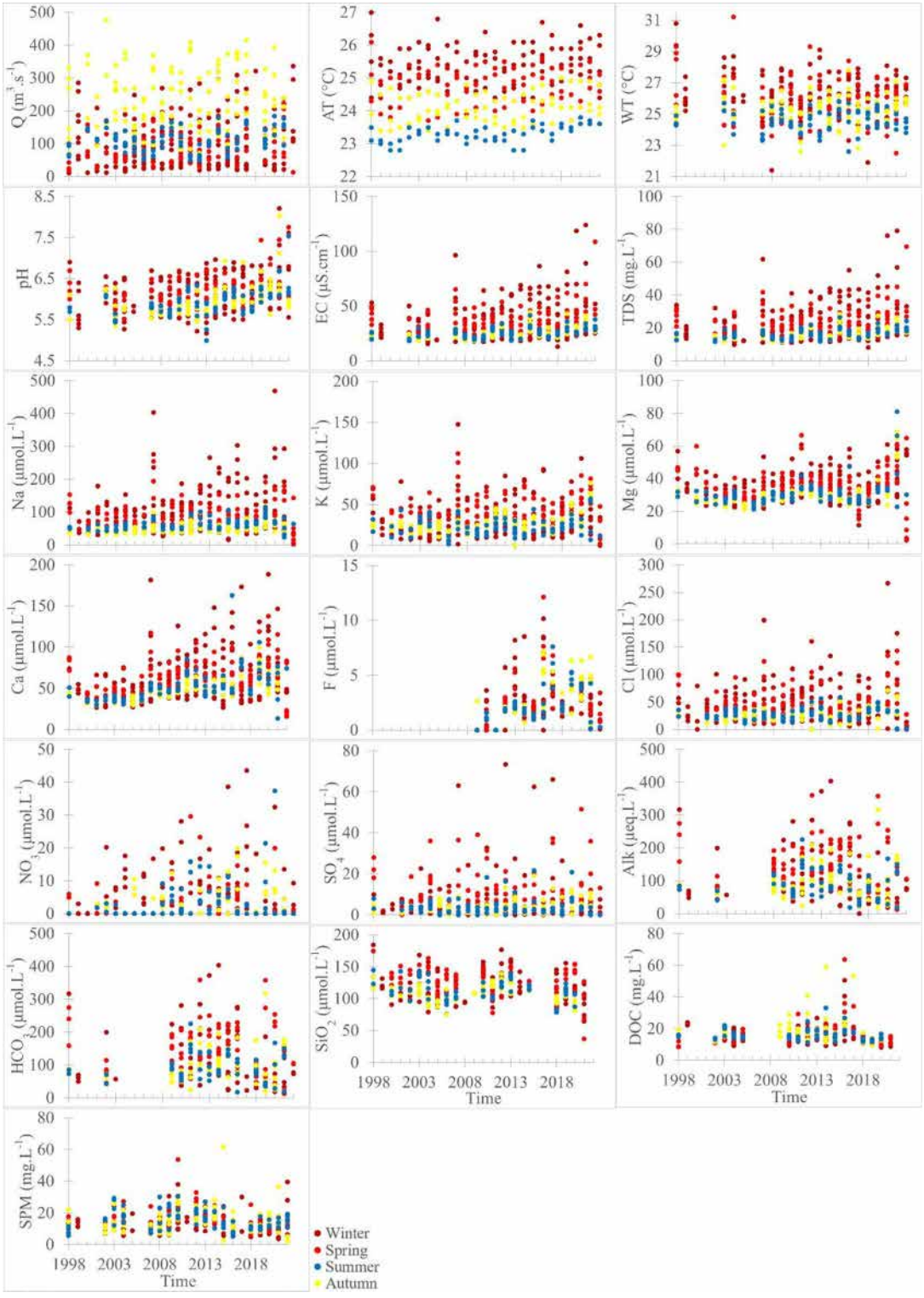

Fig. 7. Long-term fortnightly variation, depending on the seasons, for: discharge (Q), atmospheric temperature (AT), WT, pH, EC, concentrations of TDS, concentrations of major cations (Na^+, K^+, Mg^{2+}, Ca^{2+}), concentrations of major anions (F^-, Cl^-, NO_3^-, SO_4^{2-}, HCO_3^-), concentrations of SiO_2, concentrations of DOC, and concentrations of SPM at Mbalmayo station, over the period 1998–2022.

Similarly, this test applied to the long-term variation of atmospheric temperature (AT), on monthly, interseasonal and interannual base, gave p-values > 0.01 for the 5 stations. These values suggest the absence of a trend change point in the long-term evolution of Q and AT.

Long-term fortnightly variation The Modified Mann-Kendall test on the fortnightly variation in major ions concentrations indicates significant increasing trend ($p < 0.01$) in descending order of slope for: $Ca^{2+} > K^{+} > Mg^{2+} > F^{-} > NO_3^{-}$ at Olama, $Ca^{2+} > Na^{+} > K^{+} > Mg^{2+} > F^{-} > NO_3^{-}$ at Mbalmayo, $Ca^{2+} > Mg^{2+} > K^{+} > F^{-} > NO_3^{-}$ at Pont So'o, $Ca^{2+} > F^{-} > Mg^{2+} > NO_3^{-}$ at Messam, and $SiO_2 > Ca^{2+} > F^{-} > K^{+} > NO_3^{-}$ at Nsimi outlet. HCO_3^{-} and SiO_2 show significant decreasing trend ($p < 0.01$) at Olama with slope absolute value such that $HCO_3^{-} > SiO_2$. HCO_3^{-} and Cl^{-} show significant decreasing trend ($p < 0.01$) at Pont So'o and Nsimi outlet respectively. Likewise, Na^{+} and Cl^{-} show significant decreasing trend ($p < 0.01$) at Messam, with slope absolute value such that $Na^{+} > Cl^{-}$. Q shows significant increasing trend ($p < 0.01$) at Olama, Mbalmayo and Nsimi outlet, and significant decreasing trend ($p < 0.01$) at Pont So'o. AT, WT and pH generally show significant increasing trend ($p < 0.01$) for all 5 stations, except WT at Olama and Mbalmayo. EC and TDS show significant increasing trend ($p < 0.01$) at Olama, Mbalmayo and Pont So'o. Alk shows significant decreasing trend ($p < 0.01$) at Olama, Mbalmayo and Pont So'o, and SPM significant decreasing trend ($p < 0.01$) at Olama and Pont So'o.

Long-term interseasonal variation In winter, long-term variation in major ion concentrations shows significant increasing trend ($p < 0.01$) in descending order of slope for: $Ca^{2+} > K^{+} > Mg^{2+} > F^{-}$ at Olama, $Ca^{2+} > Na^{+} > K^{+} > Mg^{2+} > F^{-}$ at Mbalmayo, $Ca^{2+} > Mg^{2+} > K^{+} > F^{-}$ at Pont So'o, $Ca^{2+} > F^{-}$ at Messam, and $SiO_2 > Ca^{2+} > F^{-}$ at Nsimi outlet. SO_4^{2-} and HCO_3^{-} show significant decreasing trend ($p < 0.01$) at Olama, and HCO_3^{-} and SiO_2 show significant decreasing trend ($p < 0.01$) at Pont So'o, with slope absolute value such that $HCO_3^{-} > SO_4^{2-}$ and $HCO_3^{-} > SiO_2$, respectively. HCO_3^{-} shows significant decreasing trend ($p < 0.01$) at Mbalmayo, while the major ions show significant decreasing trend ($p < 0.01$) at Messam in a descending order of slope absolute value as follows: $SiO_2 > HCO_3^{-} > Na^{+} > Cl^{-}$. Q shows significant decreasing trend ($p < 0.01$) at Pont So'o and Nsimi outlet. AT, WT and pH generally show significant increasing trend ($p < 0.01$) for all 5 stations, except WT at Olama and Mbalmayo, and pH at Nsimi outlet. WT shows significant dereasing trend ($p < 0.01$) at Olama, and pH significant dereasing trend ($p < 0.01$) at Nsimi outlet. EC and TDS show significant increasing trend ($p < 0.01$) at Olama, Mbalmayo and Pont So'o, and significant decreasing trend ($p < 0.01$) at Nsimi outlet. Alk shows significant increasing trend ($p < 0.01$) for all 5 stations, and DOC significant decreasing trend ($p < 0.01$) at Olama and Pont So'o.

In spring, concentrations of major ions show significant increasing trend ($p < 0.01$) with a descending slope in the following order: $Ca^{2+} > F^{-} > NO_3^{-}$ at Olama, Pont So'o and Messam, $Ca^{2+} > F^{-}$ Mbalmayo, and $F^{-} > NO_3^{-}$ at Pont So'o, $F^{-} > Ca^{2+} > NO_3^{-}$ at Nsimi outlet. Concentrations of major ions show significant decreasing trend ($p < 0.01$) with a descending slope absolute value such that: $HCO_3^{-} > SiO_2 > Na^{+}$ at Pont So'o, $Na^{+} > Cl^{-} > K^{+} > SO_4^{2-}$ at Messam and $Cl^{-} > SO_4^{2-}$ at Nsimi outlet. SiO_2 shows significant decreasing trend ($p < 0.01$) at Olama and Mbalmayo. Q shows significant increasing trend ($p < 0.01$) at Olama, Mbalmayo and Messam, and AT significant increasing trend ($p < 0.01$) at Messam and Nsimi outlet. WT shows significant decreasing trend ($p < 0.01$) at Olama and significant increasing trend ($p < 0.01$) at Nsimi outlet. pH shows significant increasing trend ($p < 0.01$) for all 5 stations, and EC and TDS significant increasing trend ($p < 0.01$) at Olama and Mbalmayo. Alk shows significant decreasing trend ($p < 0.01$) at Pont So'o and SPM significant decreasing trend ($p < 0.01$) at Olama and Pont So'o.

In summer, long-term variation in major ion concentrations shows significant increasing trend ($p < 0.01$) with a descending slope in the following order: $Ca^{2+} > Na^{+} > Mg^{2+} > F^{-} > NO_3^{-}$ at Olama, $Ca^{2+} > Na^{+} > F^{-} > Mg^{2+}$ at Mbalmayo, $Ca^{2+} > Mg^{2+} > Na^{+} > K^{+} > F^{-}$ at Pont So'o, $HCO_3^{-} > Ca^{2+} > K^{+} > Mg^{2+} > F^{-} > NO_3^{-}$ at Messam, and $SiO_2 > Ca^{2+} > F^{-} > Mg^{2+} > K^{+} > SO_4^{2-} > NO_3^{-}$ at Nsimi outlet. SiO_2 shows significant decreasing trend ($p < 0.01$) at Olama and Mbalmayo, and Cl^{-} significant decreasing trend ($p < 0.01$) at Messam. Q shows significant increasing trend ($p < 0.01$) at Pont So'o and significant decreasing trend ($p < 0.01$) at Nsimi outlet. AT and pH show significant increasing trend ($p < 0.01$) for all 5 stations, and WT significant increasing trend ($p < 0.01$) at Messam and Nsimi outlet. EC and TDS show significant increasing trend ($p < 0.01$) at Olama, Mbalmayo and Pont So'o. SPM, Alk and DOC show significant decreasing trend ($p < 0.01$) at Olama, Mbalmayo and Pont So'o respectively.

In autumn, concentrations of major ions show significant increasing trend ($p < 0.01$) in descending order of slope for: $Ca^{2+} > K^{+} > Cl^{-} > Na^{+} > Mg^{2+} > F^{-} > SO_4^{2-} > NO_3^{-}$ at Olama, $Ca^{2+} > Na^{+} = K^{+} > Cl^{-} > Mg^{2+} > F^{-} > SO_4^{2-}$ at Mbalmayo, $Ca^{2+} > K^{+} > Mg^{2+} > F^{-}$ at Pont So'o, $Ca^{2+} > Mg^{2+} > F^{-}$ $K^{+} > NO_3^{-}$ at Messam, and Si > $Ca^{2+} > K^{+} > F^{-} > Mg^{2+} > NO_3^{-}$ at Nsimi outlet. HCO_3^{-} shows significant decreasing trend ($p < 0.01$) at Pont So'o, and Cl^{-} significant decreasing trend ($p < 0.01$) at Messam. AT, WT, pH, EC and TDS generally show significant increasing trend ($p < 0.01$) for all 5 stations except WT at Olama and Mbalmayo, and pH, EC and TDS at Nsimi outlet. Alk shows significant decreasing trend ($p < 0.01$) at Pont So'o, and SPM significant increasing trend ($p < 0.01$) at Messam.

Interannual and Spatial variation over the long-term Interannual and spatial variation over the long-term of discharge, physicochemical parameters and the weighted concentrations of major ions for the 5 stations is presented in Fig. 8. The result of the Modified Mann-Kendall test, applied to the long-term evolution of the interannual discharge-weighted average of the value of the physicochemical parameters and the concentration of major ions, is presented in Table S3.

The spatial variation of AT is as follows: Nsimi outlet ≈ Messam > Pont So'o ≈ Olama > Mbalmayo, suggesting a decrease in AT from tributary areas to main channel areas of the Nyong River. Almost unlike AT, WT is arranged

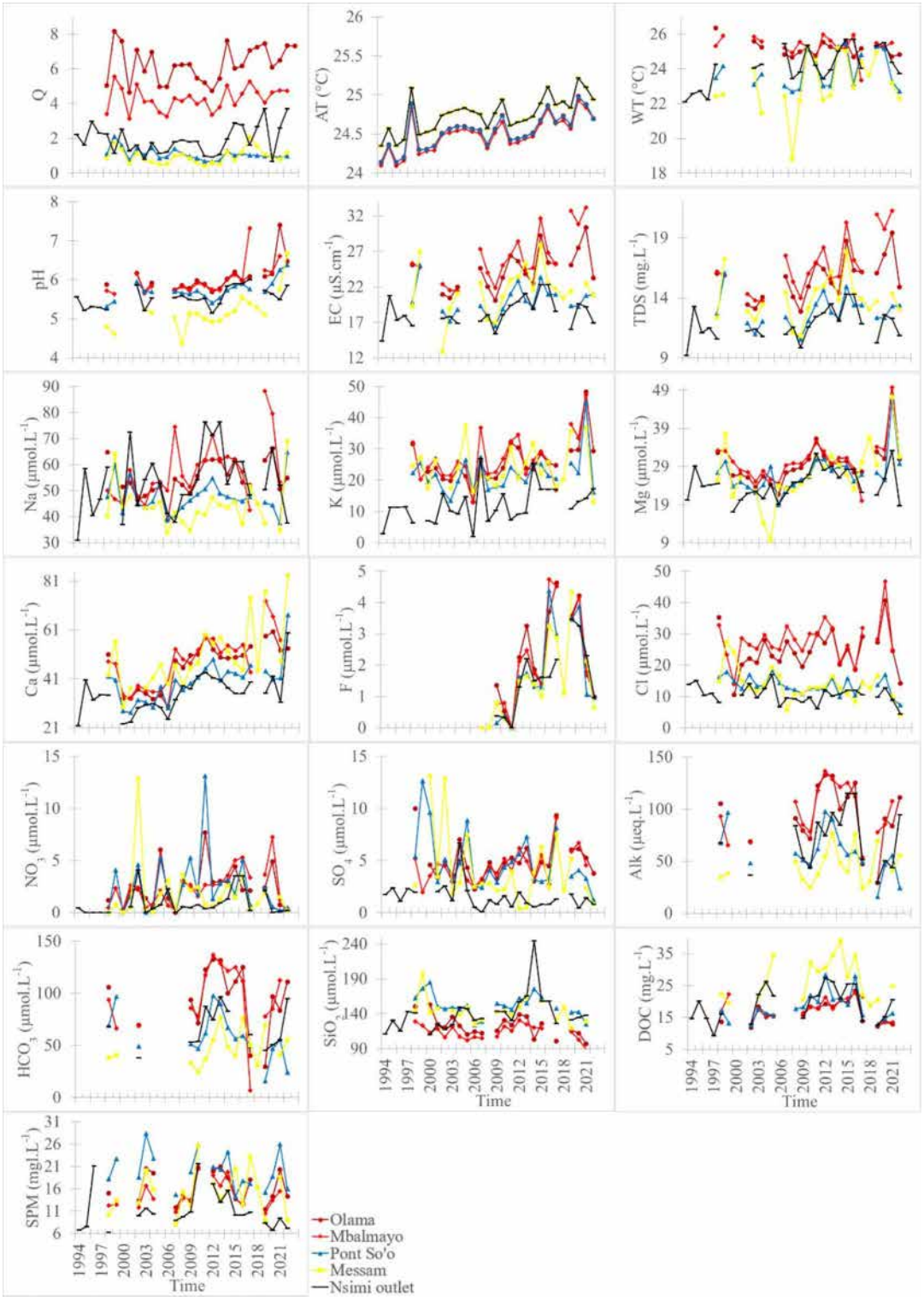

Fig. 8. Historical changes in the weighted values or concentrations of: discharge (Q), atmospheric temperature (AT), WT, pH, EC, TDS, major cations (Na^+, K^+, Mg^{2+}, Ca^{2+}), major anions (F^-, Cl^-, NO_3^-, SO_4^{2-}, HCO_3^-), SiO_2, DOC and SPM, over 1994–2022 for Nsimi outlet station, and over 1998–2022 for the Olama, the Mbalmayo, the Pont So'o, and the Messam stations. To bring Q at the same scale for all stations, it was multiplied by 10,000 for Nsimi outlet, and by 1,000 for Messam.

as follows: Mbalmayo > Olama > Nsimi outlet > Pont So'o > Messam, suggesting a general increase in WT from tributaries to the main channel.

Spatially, except Na^+, Ca^{2+}, F^-, SiO_2, DOC and SPM, all other major ions and physicochemical parameters are ranged as follows: Mbalmayo > Olama > tributary stations (Pont So'o, Messam and Nsimi outlet), suggesting that the weighted values and concentrations increase from tributaries towards the main channel of the Nyong River. On the other hand, SiO_2 and DOC showed spatial differences in an inverse order such that: tributary stations > Olama > Mbalmayo, suggesting that their concentrations decrease from tributaries towards the main channel. The major ions Na^+, Ca^{2+} and F^- did not show any discernible clear spatial differences. SPM is spatially ranged as follows: Pont So'o > Messam > Olama ≈ Mbalmayo > Nsimi outlet. The spatial variation results obtained here are generally in agreement with those on the long-term weighted averages (see above).

The annual discharge does not show a long-term trend for all stations. The variation of the annual discharge-weighted average concentrations of major ions, over the long term, shows significant increase trend ($p < 0.01$) with a descending slope in the following order: $Ca^{2+} > Na^+ = K^+ > Mg^{2+} > Cl^-$ at Olama, $Ca^{2+} > Na^+ > K^+ > F^- > Mg^{2+} > NO_3^- > SO_4^{2-}$ at Mbalmayo, $Ca^{2+} > Mg^{2+}$ at Pont So'o, $HCO_3^- = Ca^{2+} > Mg^{2+} > F^-$ at Messam and $SiO_2 > Ca^{2+} > K^+ > Mg^{2+} > F^- > NO_3^-$ at Nsimi outlet. Concentrations of major ions show significant decreasing trend ($p < 0.01$) with a descending slope absolute value such that: $HCO_3^- > Cl^- > SO_4^{2-}$ at Pont So'o and $Cl^- > SO_4^{2-}$ at Nsimi outlet. AT, pH, EC and TDS generally show significant increase trend ($p < 0.01$) for all 5 stations, except EC and TDS at Messam. WT shows significant increase trend ($p < 0.01$) at Messam and Nsimi outlet. Alk shows significant increase trend ($p < 0.01$) at Pont So'o and a significant increase at Messam.

Long-term variation in rainfall and seaward fluxes

The correlation between observed and satellite monthly rainfall data yielded a significant relationship ($p < 0.01$) with an above-average correlation coefficient ($R^2 = 0.5$; Fig. S2). This relationship validated the satellite data as representative of actual rainfall in UNB. The long-term monthly variation of solute specific fluxes is presented in Figs. 9 and 10 and S6-S8. The results of the Modified Mann-Kendall test applied on monthly and interseasonal variation of solute and SPM specific fluxes is shown in Table S4.

Exploring rainfall trend change point The Pettitt's test applied to monthly, interseasonal and interannual variation in rainfall showed p-values > 0.01, suggesting that rainfall did not change trend between 1994 and 2017 in the Nsimi outlet area, nor between 1998 and 2017 for the areas of the four other stations. In addition, the Modified Mann-Kendall test applied on rainfall (Table S4-S5) shows no significant trend ($p > 0.01$), neither on a monthly scale, nor on interseasonal and interannual scales, over the period studied, for the 5 stations. For solutes, the results of the Modified Mann-Kendall test applied to long-term variation in specific fluxes varies depending on whether observations are made monthly, interseasonally or interannually.

Long-term monthly variation The Modified Mann-Kendall test applied on the monthly variation in solutes flux indicates significant increasing trend ($p < 0.01$) in descending order of slope for: TDS > SPM > $Ca^{2+} > Na^+ > K^+ > Mg^{2+} > Cl^- > NO_3^-$ at Olama, TDS > DOC > > HCO_3^- > SPM > $Ca^{2+} > SiO_2 > Na^+ > K^+ > Cl^- > Mg^{2+} > SO_4^{2-} > F^-$ at Mbalmayo, $F^- > NO_3^-$ at Pont So'o, DOC > $SiO_2 > Ca^{2+} > Na^+ > Mg^{2+} > K^+ > F^- > Cl^- > SO_4^{2-} > NO_3^-$ at Messam, and SPM > $F^- > NO_3^-$ at Nsimi outlet. SPM and SiO_2 show significant decreasing trend ($p < 0.01$) at Pont So'o, with slope absolute value such that SPM > SiO_2.

Long-term interseasonal variation In winter, long term variation of solutes monthly flux indicates significant increasing trend ($p < 0.01$) in descending order of slope for: TDS > SPM > $Ca^{2+} > Na^+ > K^+ > F^-$ at Olama, TDS > $Ca^{2+} > Na^+ > K^+ > Cl^- > Mg^{2+} > F^-$ at Mbalmayo, and DOC > SPM > $SiO_2 > HCO_3^- > Ca^{2+} > Na^+ > K^+ > Mg^{2+} > Cl^- > SO_4^{2-} > F^-$ at Messam. Physicochemical parameters and major ions specific flux shows significant decreasing trend ($p < 0.01$) with a descending slope absolute value such that: SPM > DOC > $SiO_2 > HCO_3^-$ > TDS > Cl^- at Pont So'o and SPM > TDS > Mg^{2+} at Nsimi outlet.

In spring, solutes flux shows significant increasing trend ($p > 0.01$) with a descending slope in the following order: DOC > TDS > $HCO_3^- > Ca^{2+} > Na^+ > Cl^- > K^+ > Mg^{2+} > F^-$ at Olama, DOC > TDS > $HCO_3^- > SiO_2 > Ca^{2+} > Cl^- > Na^+ > K^+ > SO_4^{2-} > Mg^{2+} > F^-$ at Mbalmayo, $SO_4^{2-} > F^- > NO_3^-$ at Pont So'o, DOC > TDS > SPM > $HCO_3^- > Ca^{2+} > Na^+ > Mg^{2+} > K^+ > Cl^- > F^- > NO_3^-$ at Messam, and SPM > $Na^+ > F^-$ at Nsimi outlet.

In summer, solutes flux shows significant increasing trend ($p < 0.01$) with a descending slope as follows: TDS > $Ca^{2+} > F^-$ at Olama, DOC > TDS > $Ca^{2+} > Na^+ > Cl^- > Mg^{2+} > F^- > SO_4^{2-} > NO_3^-$ at Mbalmayo, $SO_4^{2-} > F^- > NO_3^-$ at Messam, and $F^- > SO_4^{2-} > NO_3^-$ at Nsimi outlet. In contrast, most solute fluxes show significant decreasing trend ($p < 0.01$) at Pont So'o with a descending slope absolute value such that: SPM > DOC > TDS > $SiO_2 > HCO_3^- > Na^+ > Cl^- > SO_4^{2-}$. In addition, F^- shows significant increasing trend ($p < 0.01$) at Pont So'o, while SiO_2 and SPM show significant decreasing trend ($p < 0.01$) at Olama and Messam respectively.

In autumn, solutes flux shows significant increasing trend ($p < 0.01$) with a descending slope in the following order: DOC > TDS > $Ca^{2+} > K^+ > Mg^{2+} = Cl^- > Na^+ > SO_4^{2-} > F^-$ at Olama, TDS > HCO_3^- > SPM > $Ca^{2+} > K^+ > Na^+ > Mg^{2+} > SO_4^{2-} > Cl^- > F^-$ at Mbalmayo, DOC > $Ca^{2+} > Mg^{2+} > F^-$ at Pont So'o, DOC > $Ca^{2+} > K^+ > Mg^{2+} > Na^+ > Cl^- > F^-$ at Messam, and DOC > SPM > $K^+ > F^- > NO_3^-$ at Nsimi outlet. Rainfall shows significant decreasing trend ($p < 0.01$) at Olama, Mbalmayo and Messam.

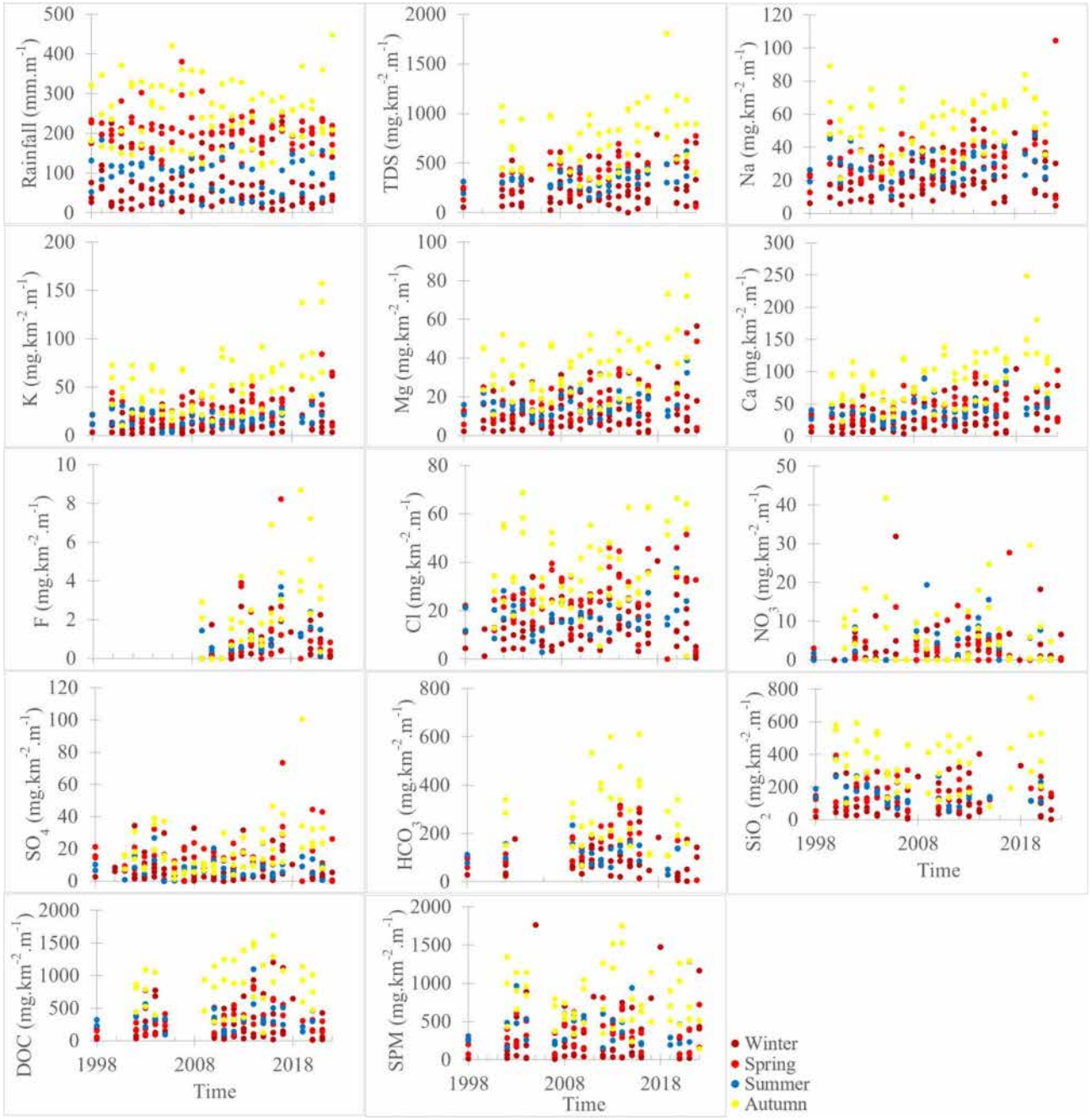

Fig. 9. Long-term monthly variation, depending on the seasons, for rainfall and specific fluxes of: TDS, major cations (Na^+, K^+, Mg^{2+}, Ca^{2+}), major anions (F^-, Cl^-, NO_3^-, SO_4^{2-}, HCO_3^-), SiO_2, DOC and SPM at Olama station, over the period 1998–2022.

Interannual and Spatial variation over the long-term Interannual and spatial variation over the long-term of rainfall and specific fluxes of TDS, major ions, DOC and SPM, for the 5 stations, is presented in Fig. 11. The results of the Modified Mann-Kendall test applied to these data are presented in Table S5.

Spatially, the results on annual rainfall heights are arranged as Olama = Pont So'o > Mbalmayo > Messam = Nsimi Outlet, suggesting a general decrease in rainfall from stations close to the Atlantic Ocean coastline to stations inland. This result is consistent with those of Olivry[46] who observed, from 40 years data (1937–1976) in the Nyong basin, that the average annual height of precipitation decreases as one moves away from the ocean. Overall, annual specific fluxes do not show any clear spatial difference, for all parameters.

Interannually, long term variation of solutes flux indicates significant increasing trend ($p < 0.01$) in descending order of slope for: TDS > Ca^{2+} > F^- at Olama, TDS > Na^+ > K^+ > NO_3^- > SO_4^{2-} > F^- at Mbalmayo, DOC > HCO_3^- > Ca^{2+} > Mg^{2+} at Messam, and DOC = HCO_3^- > SPM at Nsimi outlet. In contranst, at Pont

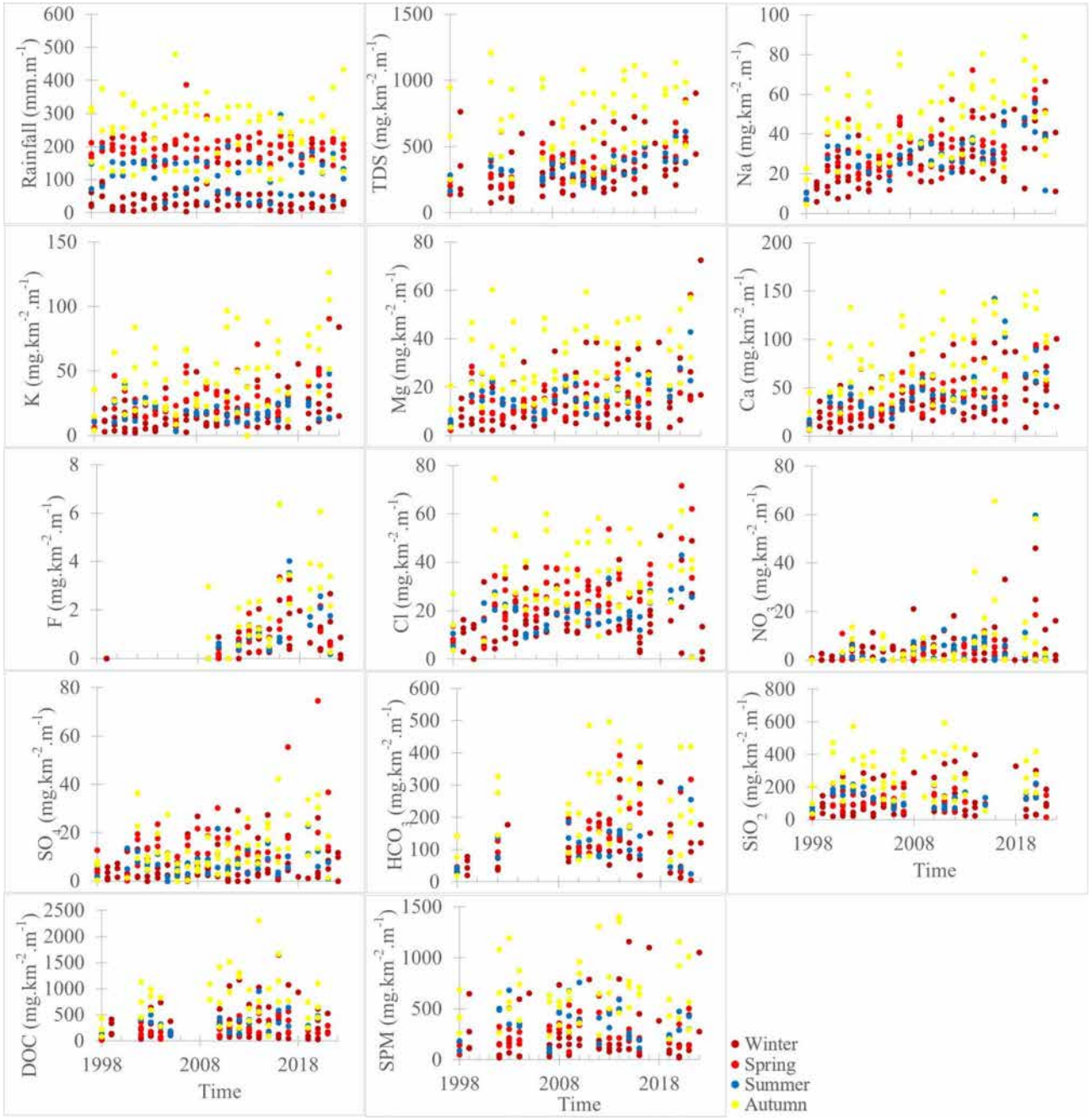

Fig. 10. Long-term monthly variation, depending on the seasons, for rainfall and specific fluxes of: TDS, major cations (Na^+, K^+, Mg^{2+}, Ca^{2+}), major anions (F^-, Cl^-, NO_3^-, SO_4^{2-}, HCO_3^-), SiO_2, DOC and SPM at Mbalmayo station, over the period 1998–2022.

So'o, solutes flux shows significant decreasing trend ($p < 0.01$) with slope absolute value such that SPM > SiO_2 > DOC > HCO_3^-.

Discussion

In the UNB, AT increases significantly ($p < 0.01$) in the long term at monthly, interseasonal and interannual scales. The interannual increase is distributed in descending order: +2.2 °C/100 years for Mbalmayo area, +2.1 °C/100 years for So'o and Nsimi areas, +2 °C/100 years for Messam area, and +1.4 °C/100 years for Olama area. Except in autumn, rainfall shows no trend ($p > 0.01$) at all-time scales and for all 5 areas. In autumn, it shows significant decreasing trend ($p < 0.01$) in Olama, Mbalmayo and Messam areas. The long-term evolution of Q contrasts with that of AT and rainfall at several points. For example, at Olama, Mbalmayo and Nsimi outlet, the significant increase ($p < 0.01$) in Q at fortnightly scale contrasts with that in AT and the absence

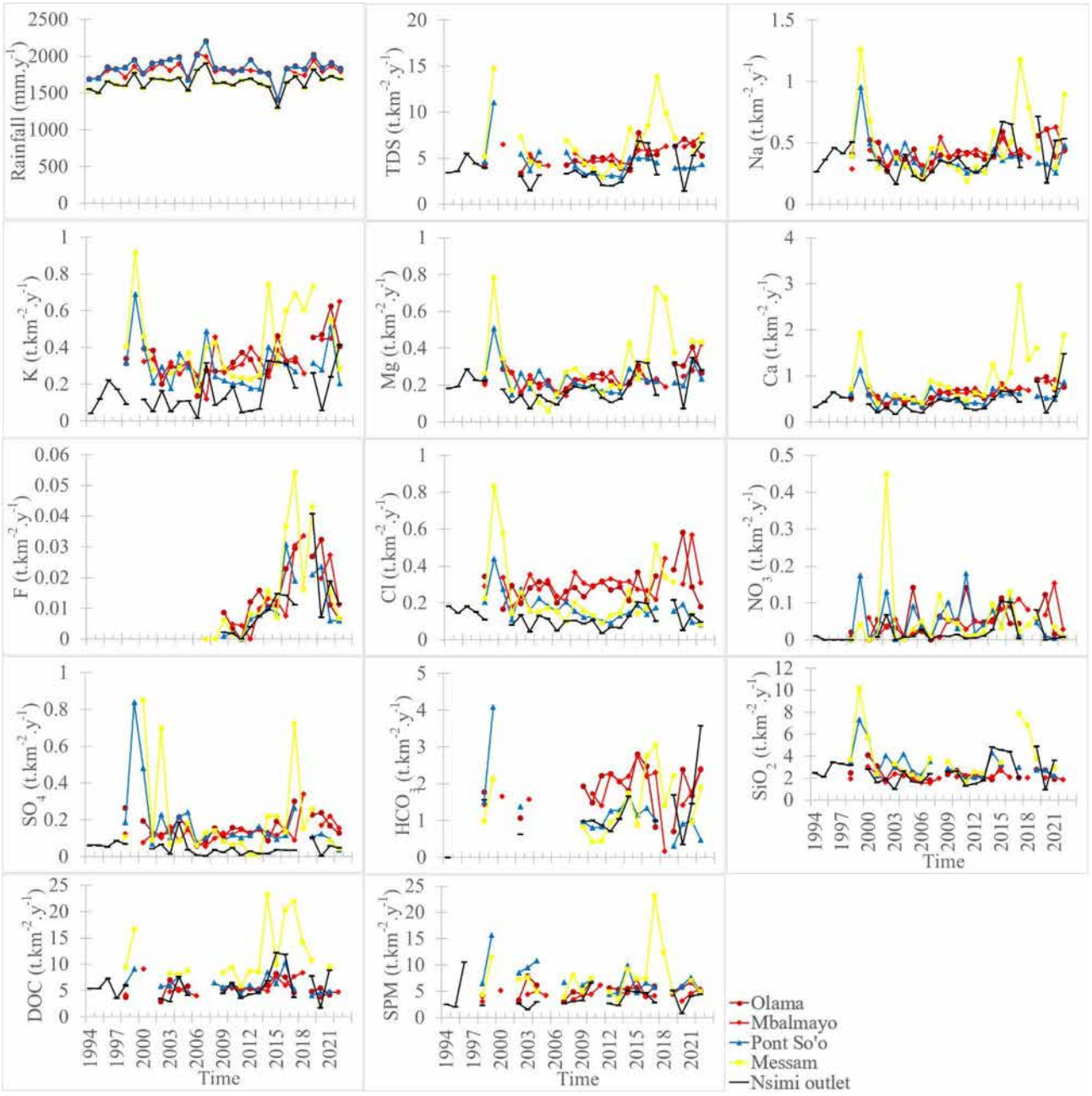

Fig. 11. Historical changes in rainfall and specific fluxes of: TDS, major cations (Na^+, K^+, Mg^{2+}, Ca^{2+}), major anions (F^-, Cl^-, NO_3^-, SO_4^{2-}, HCO_3^-), SiO_2, DOC and SPM, over 1994–2022 for Nsimi outlet station, and over 1998–2022 for the Olama, the Mbalmayo, the Pont So'o, and the Messam stations.

of trend ($p > 0.01$) in rainfall. At Olama, Mbalmayo and Nsimi outlet, the significant increase ($p < 0.01$) in spring Q contrasts with that of AT and the absence of a trend ($p > 0.01$) in rainfall. However, in tributaries, the evolution of Q at certain time scales supports the temperature effect. For example, at Pont So'o, the significant decrease ($p < 0.01$) in Q at fortnightly scale and in winter agrees with the significant increase ($p < 0.01$) in AT. Similarly, at Nsimi, the significant decrease ($p < 0.01$) in Q at fortnightly scale and in summer agrees with the significant increase ($p < 0.01$) in AT. In addition, the effect of temperature on discharge evolution is considered secondary with respect to the overall results and it is observed on certain tributaries and time scales only. On the other hand, the absence of trend and the significant increase ($p < 0.01$) observed for the discharge at the main channel stations (Mbalmayo and Olama) shows that the drinking water catchment station located in the town of Mbalmayo does not have effect on the evolution of discharge over the long term. Considering the results obtained on the evolution of rainfall and AT, the increase in discharge over the long term cannot be attributed to climate change. Thus, the only factor that can provide this explanation is the increase in impervious and agricultural surface and the decrease in forest area.

In this study, despite the significant increase in discharge, the values of pH, EC, TDS, and the concentrations of cations and anions, except Cl^-, HCO_3^-, SiO_2 and, to a lesser extent, SO_4^{2-}, significantly increase over the long term at all time scales considered. The increase in these parameters and ions eliminate discharge as a factor influencing their variation. A greater contribution of groundwater to surface water can explain the increase in the concentrations of the above parameters and ions. However, such a contribution should be accompanied by a significant decrease in the concentration of DOC over the long term. Except in spring, all stations show significant or non-significant decreasing trend in DOC over the long term. In winter, DOC shows significant decreasing trend ($p<0.01$) at Olama and Pont So'o, when the base flow is observed. In summer, DOC shows significant decreasing trend ($p<0.01$) at Pont So'o. In spring, DOC decreases non-significantly at Nsimi outlet, and increases non-significantly for the other four stations. The decrease in DOC affirms groundwater contribution to the increase in the values of the parameters pH, EC, TDS, and the concentrations of cations and anions mentioned above, over the long term. In addition to the contribution of groundwater, anthropogenic activities also influence the increase in physicochemical parameters and concentrations of major ions over the long term. Given the silicate context of the study area, the increase in pH towards a more basic character cannot be explained by the contribution of groundwater, but rather by an influence of anthropogenic activities[104]. Also, this contribution cannot explain the significant decreasing trend observed for Cl^-, HCO_3^-, SiO_2 and SO_4^{2-} concentrations.

Temporal signature of LULCC and population growth on Nyong river chemistry

LULCC in the UNB results in a replacement of forest and water areas by impervious and agricultural surface. These changes can be attributed to two types of factors: (1) direct factors related to economic profit and (2) indirect factors associated with population increase[105]. Direct factors include large-scale commercial agriculture (cocoa, palm, coffee) and industrial selective logging. Indirect factors are justified by significative high correlation between LULC classes and population, which is the origin of impervious and agricultural surface expansion through: energy supply, small-scale agriculture for survival (banana, plantain, cassava, peanuts, macabo, etc.), bush fires and the construction of roads and houses for housing and commerce. Bushfires are used to kill trees to create space for crops.

Increases in population and LULCC affect water chemistry in UNB. Like all Cameroonian cities, the localities of the UNB do not have a waste and wastewater management or sanitation system. The waste and wastewater generated increases with the population and it is dumped into the environment and river without control or prior treatment. In addition, the septic tanks are leached towards the river. The increase in impervious and agricultural surface and associated activities is accompanied by an ever-increasing use of agricultural inputs (fertilizers, pesticides, fungicide and herbicides), which can deteriorate water quality. Waste and wastewater also result from activities such as breweries, commerce, livestock farming, fishing, etc. The waste and wastewater produced increase the pollution load in the environment.

Several factors related to LULCC could explain the evolution of elemental concentrations and fluxes over the long term. The significant increase in the concentration of Na^+ can be attributed to the release of untreated domestic salts into the environment, as observed in the Mekong basin[106]. The application of potassium chloride fertilizers in agricultural production is a potential source of the significant increase in K^+. The increase in Ca^{2+} can be associated with waste and wastewater from various industries. F^- can be attributed to the application of inorganic phosphate fertilizers, pesticides and industrial wastes[104]. The increase in NO_3^- can be associated to open defecation, LULCC, chemical fertilizers, animal waste materials, and untreated sewage resulting from industrial and domestic waste[104]. Generally, for the five stations, and consistently with increasing concentrations and discharge, specific fluxes to the sea increase significantly with time for Na^+, K^+, Mg^{2+}, Ca^{2+}, F^-, Cl^- and NO_3^-.

The overall significant decrease observed for Cl^-, SO_4^{2-}, Alk, HCO_3^-, and SiO_2, may be associated with increased photosynthetic activity due to eutrophication of the Nyong River[107]as well as slash-and-burn cultivation. Aquatic phytoplankton (e.g., diatoms) assimilate dissolved inorganic carbon and nutrients (e.g., N, P, SiO_2) to synthesize organic compounds[108]. High N and P loads introduced by human activities into the environment and the river boost photosynthetic activity and consequently increase primary production, resulting in a significant decrease in the value of Alk and concentrations of Cl^-, SO_4^{2-}, HCO_3^- and SiO_2. This result is consistent with what has been observed in the Mekong River[106] and the Yangtze River[109]but it is contrast to what has been observed in the Mississippi River[110]. Slash-and-burn agriculture is a common practice in the Nyong, and was expected to influence river water chemistry over the long-term[85,111]. Indeed, many experimental studies have shown that the first rains following slash-and-burn lead to an increase in the concentration of elements in the water for a few hours to a few days, before falling back to or below the pre-burn level[112–114]. In the UNB, this practice probably leads to the release of cations and anions which are leached by the first rains from February to March. In the long term, this release leads to the depletion of these chemical elements in the soil, hence the significant decrease ($p<0.01$) observed for Cl^-, SO_4^{2-}, Alk, HCO_3^-, and SiO_2. The significant increase ($p<0.01$) in cations and NO_3^- suggests that losses from slash-and-burn are lower than inputs from domestic and industrial waste, as well as agricultural inputs. On the other hand, the significant decrease ($p<0.01$) in Cl^-, SO_4^{2-}, Alk, HCO_3^-, and SiO_2 suggests that losses from photosynthesis and slash-and-burn must be greater than contributions from other processes and factors. A third factor that could explain the variation in SiO_2 concentration is a change in the rate of chemical and physical weathering over time[106]. Indeed, a decrease in the weathering rate over the long term should lead to a decrease in SiO_2 concentration, and vice versa[106]. However, the deforestation in the Nyong basin, as shown in this study, is likely to accelerate weathering over time[115,116]. Thus, this third hypothesis is rather unlikely. In addition to the greater contribution of groundwater discussed earlier (see Sect. 5.1), the significant ($p<0.01$) long-term decrease in DOC can also be associated with slash-and-burn. This leads to volatization/oxidation by fire of organic litter, which generally contributes to the DOC

content in the water[113]. In the long term, this volatization/oxidation can lead to a decrease in organic litter in the Basin and, therefore, in DOC in the river water. Significant decreasing trend ($p<0.01$) in SPM was observed at Olama at the fortnightly scale, in spring and summer, as well as at Pont So'o at the fortnightly and interannual scales and in spring. At Pont So'o, the decreasing in SPM was estimated at −0.3 $\mathrm{mg.L^{-1}}.y^{-1}$, and it reflects a lowering in physical erosion, despite the increase in impervious and agricultural surface.

Some parameters and ions showed fluxes whose trends contrasted with those of their original concentrations at monthly, interseasonal and annual scales. This is the case for $\mathrm{Cl^-}$, $\mathrm{HCO_3^-}$, $\mathrm{SiO_2}$ DOC, SPM and, to a lesser extent, $\mathrm{SO_4^{2-}}$. Indeed, these parameters and ions generally showed concentrations whose general trends decreased significantly ($p<0.01$) or not ($p>0.01$) over the long term (see Sect. 4.6.2). However, the general trends of their fluxes increased significantly ($p<0.01$) or not ($p>0.01$) over the long term (see Sect. 4.6.3). This contrast is linked to the significant ($p<0.01$) increase or not ($p>0.01$) over the long term of the corresponding discharge used to calculate the fluxes.

Spatial signature of "LULC and population" distribution on Nyong river chemistry

The spatial variation of water chemistry in the Nyong River shows that it is influenced by LULC composition and population density. Indeed, pH, EC, Alk and major ions show higher average values on the stations of the main channel of the Nyong River (Mbalmayo and Olama) compared to the stations of the tributaries. In addition, the Mbalmayo station displays average concentrations of physicochemical parameters and major ions that are generally higher than those of all stations. The high average values of parameters in Mbalmayo station and Nyong are linked to a high relative population density and impervious and agricultural surface in the city of Yaounde. Yaounde located in Mfoundi Division, is the main city of Nyong and one of the two largest cities in Cameroon. Projections show that the population of Yaounde in 2020 was 3,317,436. Covering an area of 180 $\mathrm{km^2}$ (0.9% of the total area of the UNB), Yaounde is host 80.6% of the population of the Nyong basin. The proportion of the area of Yaounde is therefore marginal compared to that of the sheltered population. The waste and wastewater generated by the high population density and industries explains the high values of physicochemical parameters and major ions in Mbalmayo and Olama compared to the tributaries.

Limits and perspectives of the study

This study has several limitations related to: (1) Landsat data, (2) climate data, and (3) the population projection model.

For the LULCC study, Landsat images offer several advantages, namely: their continuous and consistent recording from 1972 to the present day, their global coverage and repeatability, and their free, open, and public access. Their moderate resolution of 30 m is also suitable for studying the temporal evolution of the forest, impervious and agricultural surface in a watershed the size of the Nyong. However, this resolution remains too high to study the evolution of the water surface, which is marginal compared to forest and impervious and agricultural surface. Thus, for a proper study of the evolution of the water surface, 1 m high-resolution data (for example) would be more suitable. However, such data have limited access and are subject to a charge. In addition, such data are recent and therefore do not offer the possibility of studying LULCC over the long term as Landsat data. In addition to resolution, the cloud cover of the Landsat scenes was also a limitation in this study. For example, to create the 2010 LULC map, scenes from 2010, 2011, and 2013 had to be combined (Table 1) due to cloud cover. Thus, the LULCC was necessarily underestimated between 2010 and 2015.

The limitations of climate data lie in both their validity and their spatial resolution. The correlation between observed and satellite data yielded a correlation coefficient of 0.5, suggesting only moderate validity. Based on the spatial resolution of the climate data (0.5°×0.5°), Pont So'o and Olama stations, as well as those of Messam and Nsimi outlet, fell into the same grids. This suggests similar rainfall patterns in the areas of these stations. Although there are no observational data that could confirm or refute this similarity, higher-resolution satellite data could have dispelled any doubt.

The population projection model estimated that the population continued to evolve perfectly as in the past. However, this model suffers from the lack of census data that could allow inclusion of fit statistics and uncertainty quantification. Furthermore, the model also does not take into account internal displacement caused by the security crisis that began in 2016 in the North West and South West regions of Cameroon. Indeed, this crisis led to a significant displacement of populations fleeing insecurity from these regions to other parts of the country. The localities of UNB, and mainly Yaoundé, were necessarily impacted by this displacement, receiving a significant influx of population. This influx likely led to an above-average population growth rate from 2016 onwards.

UNB is the only critical zone of the Central African rainforest with 29 years of hydrological and hydrochemical data. This long-term monitoring has highlighted a significant change in river chemistry and, to a lesser extent, in discharge. This change has been attributed to anthropogenic forcing, notably the conversion of forest to impervious and agricultural land. However, a more comprehensive, robust, and reliable understanding of the functioning of the critical zone would be possible by adding: (1) climate observational data, (2) groundwater data, and (3) very high frequency data. In fact, using of satellite climate data has made it possible to link river chemistry to climate. However, regular monitoring of climate parameters (rainfall, AT, air relative humidity, wind velocity and direction, and global radiation) corresponding to hydrological and hydrochemical data, would allow for more robust and reliable conclusions on the role of climate in water chemistry. In addition to the river, acquiring the same data on groundwater (water level and hydrochemical data) would allow an analysis of the existing interaction between the two compartments. Daily, fortnightly and monthly data already provide a good basis for modelling UNB functioning. For example, using part of the data used here, Komba et al.[104] developed a model to predict river chemistry from discharge. However, very high-frequency data (minute to hourly scale) would allow for better validation and calibration of the model.

Conclusion

This study aimed to examine how hydroclimatic factors, demographic growth, and LULCC interact to affect river chemistry in the UNB, a critical humid tropical ecosystem in Central Africa. The results show that between 2005 and 2020, the population increased in UNB from 2.6 million to 4.1 million. This population growth has created demands such as food, housing, agricultural activities, etc. To meet these demands, populations have converted 1,207 km^2 of forest into impervious and agricultural surface (buildings, roads, agricultural land, etc.). LULC for forest, impervious and agricultural surface, and water changed as from 2005 to 2020: 17,845 km^2 to 16,638 km^2 (−6.7%), 1,376 km^2 to 2,587 km^2 (+88%), and 15 km^2 to 11 km^2 (−26.7%), respectively. Increase in impervious and agricultural surface increased soil sealing, thus promoting increase runoff and discharge, in the long term. Despite the discharge increase, the discharge of household and industrial waste and wastewater into the environment and river led to significant increase ($p < 0.01$) in pH, EC, TDS, cation and NO_3^- concentrations. Also, it could be due to a greater contribution of groundwater to surface water, as supported by the significant decrease ($p < 0.01$) in DOC over the long term. The significant decrease in Cl^-, SO_4^{2-}, Alk, HCO_3^-, and SiO_2 was associated with increased photosynthetic activity due to eutrophication of the Nyong River, as well as long term depletion of these chemical elements in the soil by slash-and-burn agriculture. Besides the contribution of groundwater, the significant decrease ($p < 0.01$) in DOC was also associated with slash-and-burn agriculture which leads to volitization/oxidation of the organic litter that causes it. The significant decrease in SPM ($p < 0.01$) reflects a decrease in physical impairment in UNB.

At the end of this study, the following recommendations are made for sustainable management of the UNB:

(1) Continue current monitoring to have longer hydrological and hydrochemical observations series;
(2) Combine this monitoring with observations of climate parameters, groundwater level and chemistry, and hydrological and hydrochemical observations on a minute to hourly scale;
(3) Provide the towns in the basin with a system for collecting, recycling and treating the waste and wastewater produced, before releasing them into the environment;
(4) establish a policy for the choice and quantification of agricultural inputs used;
(5) Mitigatedeforestation by reducing the timber trade.

Data availability

All data presented in this manuscript can be accessed freely from the three DOIs below: https://doi.org/10.6096/BVET.CMR.HYDROhttps://doi.org/10.6096/BVET.CMR.METEOhttps://doi.org/10.6096/BVET.CMR.HCHEM.

Received: 8 April 2025; Accepted: 10 July 2025
Published online: 29 July 2025

References

1. Genet, A. Population growth and land use land cover change scenario in Ethiopia. *Int. J. Environ. Prot. Policy*. **8**, 77–85. https://doi.org/10.11648/j.ijepp.20200804.12 (2020).
2. Assede, E. S. P. et al. Understanding drivers of land use and land cover change in africa:a review. *Curr. Landsc. Ecol. Rep.* **8**, 62–72. https://doi.org/10.1007/s40823-023-00087-w (2023).
3. Olorunfemi, I. E., Olufayo, A. A., Fasinmirin, J. T. & Komolafe, A. A. Dynamics of land use land cover and its impact on carbon stocks in Sub-Saharan africa: an overview. *Environ. Dev. Sustain.* **24** https://doi.org/10.1007/s10668-021-01484-z (2021).
4. Olorunfemi, I. E., Fasinmirin, J. T., Olufayo, A. A. & Komolafe, A. A. GIS and remote sensing—Based analysis of the impacts of land use/land cover change (LULCC) on the environmental sustainability of Ekiti-State, South-western Nigeria. *Environ. Dev. Sustain.* **22**, 661–692. https://doi.org/10.1007/s10668-018-0214-z (2018).
5. Rudel, T. K. The National determinants of deforestation in sub-Saharan Africa. *Philosophical Trans. Royal Soc. B.* **368**, 20120405. https://doi.org/10.1098/rstb.2012.0405 (2013).
6. Pandey, B. K., Khare, D., Kawasaki, A. & Meshesha, T. W. Integrated approach to simulate hydrological responses to land use dynamics and climate change scenarios employing scoring method in upper Narmada basin. *India J. Hydrology*. **598**, 126429. https://doi.org/10.1016/j.jhydrol.2021.126429 (2021).
7. Tan, M. L., Ibrahim, A. L., Yusop, Z., Duan, Z. & Ling, L. Impacts of land-use and climate variability on hydrological components in the Johor river basin, Malaysia. *Hydrol. Sci. J.* **60**, 873–889. https://doi.org/10.1080/02626667.2014.967246 (2015).
8. Obahoundje, S. et al. Assessment of Spatio-Temporal Changes of Land Use and Land Cover over South-Western African Basins and Their Relations with Variations of Discharges. Hydrology 5, 56; (2018). https://www.mdpi.com/2306-5338/5/4/56
9. Araza, A., Perez, M., Cruz, R. V., Aggabao, L. F. & Soyosa, E. Probable streamflow changes and its associated risk to the water resources of Abuan watershed, Philippines caused by climate change and land use changes. *Stoch. Env. Res. Risk Assess.* **35**, 389–404. https://doi.org/10.1007/s00477-020-01953-3 (2021).
10. Gomes, L. C. et al. Disentangling the historic and future impacts of land use changes and climate variability on the hydrology of a mountain region in Brazil. *J. Hydrol.* **594**, 125650. https://doi.org/10.1016/j.jhydrol.2020.125650 (2021).
11. Kayitesi, N. M., Guzha, A. C. & Mariethoz, G. Impacts of land use land cover change and climate change on river hydro-morphology- a review of research studies in tropical regions. *J. Hydrol.* **615**, 128702. https://doi.org/10.1016/j.jhydrol.2022.128702 (2022).
12. Nkhoma, L., Ngongondo, C., Dulanya, Z. & Monjerezi, M. Evaluation of integrated impacts of climate and land use change on the river flow regime in Wamkurumadzi river, Shire basin in Malawi. *J. Water Clim. Change*. **12** https://doi.org/10.2166/wcc.2020.138 (2020).
13. Yifru, B. A., Chung, I. M., Kim, M. G. & Chang, S. W. Assessing the effect of land/use land cover and climate change on water yield and groundwater recharge in East African rift Valley using integrated model. *J. Hydrology: Reg. Stud.* **37**, 100926. https://doi.org/10.1016/j.ejrh.2021.100926 (2021).
14. Raihan, F., Ondrasek, G., Islam, M. S., Maina, J. M. & Beaumont, L. J. Combined impacts of climate and land use changes on Long-Term streamflow in the upper Halda basin. Bangladesh. *Sustainability* **13** (21), 12067 (2021). https://www.mdpi.com/2071-1050/13/21/12067
15. Tan, X. et al. Impacts of climate change and land use/cover change on regional hydrological processes: case of the Guangdong-Hong Kong-Macao greater Bay area. *Front. Environ. Sci.* **9**, 783324. https://doi.org/10.3389/fenvs.2021.783324 (2022).

16. Kumar, M., Denis, D., Kundu, A., Joshi, N. & Suryavanshi, S. Understanding land use/land cover and climate change impacts on hydrological components of Usri watershed. India. *Appl. Water Sci.* **12**, 39. https://doi.org/10.1007/s13201-021-01547-6 (2022).
17. Harifidy, R. Z. et al. Assessing future intra-basin water availability in madagascar: accounting for climate change, population growth, and land use change. *Water Res.* **257**, 121711. https://doi.org/10.1016/j.watres.2024.121711 (2024).
18. Bekele, D., Alamirew, T., Kassa, A., Zeleke, G. & Melesse, A. Modeling the impacts of land use and land cover dynamics on hydrological processes of the Keleta watershed. *Ethiopia Environ. Hazards*. **18**, 246–265. https://doi.org/10.1080/17477891.2018.1561407 (2018).
19. Näschen, K. et al. The impact of land use/land cover change (LULCC) on water resources in a tropical catchment in Tanzania under different climate change scenarios. *Sustainability* **11**, 12, 7083. https://doi.org/10.3390/su11247083 (2019).
20. Teklay, A., Dile, Y. T., Asfaw, D. H., Bayabil, H. K. & Sisay, K. Impacts of climate and land use change on hydrological response in Gumara watershed. *Ethiopia Ecohydrology Hydrobiol.* **21**, 2, 315–332. https://doi.org/10.1016/j.ecohyd.2020.12.001 (2021).
21. Naha, S., Rico-Ramirez, M. A. & Rosolem, R. Quantifying the impacts of land cover change on hydrological responses in the Mahanadi river basin in India. *Hydrol. Earth Syst. Sci.* **25**, 12, 6339–6357. https://doi.org/10.5194/hess-25-6339-2021 (2021).
22. Chen, J. S. et al. Spatial and Temporal analysis of water chemistry records (1958–2000) in the Huanghe (Yellow River) basin. *Glob Biogeochem. Cycles*. **19** https://doi.org/10.1029/2004GB002325 (2005). GB3016.1–GB3016.24.
23. Birhanu, A., Masih, I., van der Zaag, P., Nyssen, J. & Cai, X. Impacts of land use and land cover changes on hydrology of the Gumara catchment, ethiopia. Physics and chemistry of the Earth. *Parts A/B/C.* **112**, 165–174. https://doi.org/10.1016/j.pce.2019.01.006 (2019).
24. Ansari, A., Sen, I. S. & Sinha, R. Trends of water composition and discharge in the Ramganga river, Ganga basin over the last 40 years signal enhanced nitrate flux. *J. Hydrol.* **641**, 131822. https://doi.org/10.1016/j.jhydrol.2024.131822 (2024).
25. Delaffon, V. P. et al. Long and short-term trends of stream hydrochemistry and high frequency surveys as indicators of the influence of climate change, agricultural practices and internal processes (Aurade agricultural catchment, SW France). *Ecol. Ind.* **110** https://doi.org/10.1016/j.ecolind.2019.105894 (2019).
26. Zhang, S. R. et al. Water chemistry of the Zhujiang (Pearl River): Natural processes and anthropogenic influences. *J. Phys. Res.* **112**, F01011. https://doi.org/10.1029/2006JF000493 (2007).
27. Chen, J. S., Wang, F. Y., Xia, X. H. & Zhang, L. T. Major element chemistry of the Changjiang (Yangtze River). *Chem. Geol.* **187**, 231–255. https://doi.org/10.1016/S0009-2541(02)00032-3 (2002).
28. Probst, J. L. Nitrogen and phosphorous exportation in the Garonne basin (France). *Hydrology* **76**, 281–305. https://doi.org/10.1016/0022-1694(85)90138-6 (1985).
29. Wels, C., Cornett, R. J. & Lazerte, B. D. Hydrograph separation: a comparison of geochemicaland isotopic tracers. *J. Hydrol.* **122** (1–4), 253–274. https://doi.org/10.1016/0022-1694(91)90181-G (1991).
30. Ladouche, B. et al. Hydrograph separation using isotopic, chemical and hydrological approaches (Strengbach catchment, France). *J. Hydrol.* **242**, 255–274. https://doi.org/10.1016/S0022-1694(00)00391-7 (2001).
31. Kpoumié, A. et al. Spatio-temporal assessing rainfall and dam impacts on surface runoff in the Sanaga river basin (transition tropical zone in central part of Cameroon). *Sustainable Water Resour. Manage.* **8**, 26. https://doi.org/10.1007/s40899-022-00624-1 (2022).
32. Ewane, E. B. & Lee, H. H. Assessing land use/land cover change impacts on the hydrology of Nyong river basin, Cameroon. *J. Mountain Sci.* **17** (1), 50–67. https://doi.org/10.1007/s11629-019-5611-8 (2020).
33. Ebodé, V. B., Mahé, G. & Amoussou, E. Changement climatique Dans Le Bassin versant de l'ogooué: évolution récente et impact Sur Les écoulements. *Proc. Int. Association Hydrol. Sci.* **384**, 247–253. https://doi.org/10.5194/piahs-384-247-2021 (2021).
34. Ebodé, V. B. et al. Impact of rainfall variability and land use change on river discharge in South Cameroon. *Water* **14**, 941. https://doi.org/10.3390/w14060941 (2022).
35. Ewane, E. B. Assessing land use and landscape factors as determinants of water quality trends in Nyong river basin, Cameroon. *Environ. Monit. Assess.* **192**, 507. https://doi.org/10.1007/s10661-020-08448-2 (2020).
36. Mediebou, C. & Otsomotsi Mbida, A. M. Dynamiques spatiales et mobilités à Akonolinga (Cameroun). *Eur. Sci. J.* **17**, 81. https://doi.org/10.19044/esj.2021.v17n28p81 (2021).
37. Mingang, D. L., Ngueguim, J. R., Momo, S. C., Tchongouang, A. & Tientcheu, T. A. *L. Quantifying Forest Loss in the Mbalmayo Forest Reserve* (Center Region, Cameroon), 2022). https://doi.org/10.4236/gep.2022.109016
38. Kamran, K. J. A., Khayyam, U., Waheed, A. & Khokhar, M. F. Exploring the nexus between land use land cover (LULC) changes and population growth in a planned City of Islamabad and unplanned City of Rawalpindi. *Pakistan Heliyon*. **9**, e13297. https://doi.org/10.1016/j.heliyon.2023.e13297 (2023).
39. Khan, N., Raza, M., Shakoor, M. S. A., Biswas, F. & Rahaman, M. Dynamic of population growth and its effect on land use/land cover of Bahraich district in Uttar Pradesh. *J. Environ. Stud. Sci.* https://doi.org/10.1007/s13412-022-00805-6 (2022).
40. Ahearn, D. S. et al. Land use and land cover influence on water quality in the last free-flowing river draining the Western Sierra nevada, California. *J. Hydrol.* **313**, 234–247. https://doi.org/10.1016/j.jhydrol.2005.02.038 (2005).
41. Li, S., Gu, S., Liu, W., Han, H. & Zhang, Q. Water quality in relation to land use and land cover in the upper Han river basin, China. *Catena* **75**, 216–222. https://doi.org/10.1016/j.catena.2008.06.005 (2008).
42. Liu, Z., Wang, Y., Li, Z. & Peng, J. Impervious surface impact on water quality in the process of rapid urbanization in shenzhen, China. *Environ. Earth Sci.* **68**, 2365–2373. https://doi.org/10.1007/s12665-012-1918-2 (2013).
43. Bu, H., Meng, W., Zhang, Y. & Wan, J. Relationships between land use patterns and water quality in the Taizi river basin, China. *Ecol. Ind.* **41**, 187–197. https://doi.org/10.1016/j.ecolind.2014.02.003 (2014).
44. Chen, D., Elhadj, A., Xu, H., Xu, X. & Qiao, Z. A study on the relationship between land use change and water quality of the Mitidja watershed in Algeria based on GIS and RS. *Sustainability* **12**, 3510. https://doi.org/10.3390/su12093510 (2020).
45. Aubreville, A. Climats, forêts et désertification de l'Afrique Tropicale. Paris, Larousse (1959).
46. Olivry, J. C. Fleuves et rivières du Cameroun. Collection, Monographies Hydrologiques ORSTOM, 733p (1986).
47. Nkoue Ndondo, G. R. *Le Cycle Du Carbone En Domaine Tropical Humide: Exemple Du Bassin Versant Forestier Du Nyong Au Sud Cameroun* (Doctorat de l'Université de Toulouse et PhD de l'Université de Yaoundé I, 2008).
48. Moustapha, M. et al. Partitioning carbon sources between wetland and well-drained ecosystems to a tropical first-order stream - Implications for carbon cycling at the watershed scale (Nyong, Cameroon). *Biogeosciences* **19**, 137–163. https://doi.org/10.5194/bg-19-137-2022 (2022).
49. Laclavère, G. & Loung, J. F. Les atlas afrique. République unie du Cameroun. *Ed. Jeune Afrique*, 72 (1973).
50. Santoir, C. & Bopda, A. Atlas régional Sud-Cameroun. *Ed. ORSTOM*, 53 (+ 21 planches. 2-7099-1271-6 (1995).
51. Nzenti, J. P., Barbey, P., Macaudiere, J. & Soba, D. Origin and evolution of the late precambrian high-grade Yaoundé gneisses (Cameroon). *Precambrian Res.* **38**, 91–109. https://doi.org/10.1016/0301-9268(88)90086-1 (1988).
52. Stendal, H. et al. Derivation of detrital rutile in the Yaounde region from the neoproterozoic Pan-African belt in Southern Cameroon (Central Africa). *J. Afr. Earth Sc.* **44**, 443–458. https://doi.org/10.1016/j.jafrearsci.2005.11.012 (2006).
53. Owona, S. et al. PanAfrican metamorphic evolution in the Southern Yaounde group (Oubanguide complex, Cameroon) as revealed by EMP-Monazite dating and thermobarometry and Garnet metapelites. *J. Afr. Earth Sc.* **59**, 125–139. https://doi.org/10.1016/j.jafrearsci.2010.09.003 (2011).
54. Yonta-Ngouné, C. et al. Geological context of the Boumnyebel talcschists (Cameroun): inferences on the PanAfrican belt of central Africa. *C.R. Geosci.* **342**, 108–115. https://doi.org/10.1016/j.crte.2009.12.007 (2010).

55. Metang, V. et al. Petrography and geochemistry of metasedimentary rocks from the Southwestern portion of the Yaounde group in cameroon: provenance and tectonic implications. *Earth Sci.* **11**, 232–249. https://doi.org/10.1007/s11631-023-00630-w (2022).
56. Chombong, N. N. et al. Host rock geochemistry, texture and chemical composition of magnetite in iron ore in the Neoarchaean Nyong unit in Southern Cameroon. *Appl. Earth Sci.* **126**, 129–145. https://doi.org/10.1080/03717453.2017.1345507 (2017).
57. Maurizot, P., Abessolo, A., Feybesse, J. L. & Johan, L. P. Etude de prospection minière du Sud-Ouest cameroun. Synthèse des travaux de 1978 à 1985. *Rapport De BRGM*. **85**, 274 (1986).
58. Owona, S. et al. New igneous (zircon Pb/Pb) and metamorphic (Rb/Sr) ages in the neoproterozoic Yaounde group (Cameroon, central Africa): Consequences for the orogenic evolution north of The Congo Craton. *Int. J. Earth Sci.* **101**, 1689–1703. https://doi.org/10.1007/s00531-012-0751-x (2012).
59. Penaye, J. et al. The 2.1 Ga West central African belt in cameroon: extension and evolution. *J. Afr. Earth Sci.* **39**, 159–164. https://doi.org/10.1016/j.jafrearsci.2004.07.053 (2004).
60. Shang, C. K. et al. Major and trace element geochemistry, Rb–Sr and Sm–Nd systematics of TTG magmatism in the congo craton: case of the Sangmelima region, Ntem complex, Southern Cameroon. *J. Afr. Earth Sc.* **40**, 61–79. https://doi.org/10.1016/j.jafrearsci.2004.07.005 (2004).
61. Pouclet, A. et al. Archaean crustal accretion at the Northern border of the congo craton (South Cameroon), The charnockite TTG link. *Bull. Geol. Soc. France*. **178**, 331–342. https://doi.org/10.2113/gssgfbull.178.5.331 (2007).
62. Food and Agricultural Organization of the United Nations (FAO). *State of the World's Forests* (Food and Agriculture Organization of the United Nations, 2007).
63. Ministry of Economy and Finance/World Bank (MINEFI). *Living Conditions and Poverty Profile in Cameroon in 2001 – Final Results* (Yaounde, 2002).
64. Gbetnkom, D. Deforestation in cameroon: immediate causes and consequences. *Environ. Dev. Econ.* **0**, 557–572. https://doi.org/10.1017/S1355770X05002330 (2005).
65. Besong, B. J. et al. 'New directions in National Forestry policies – Cameroon in Cleaver (eds). Conservation of West and Central African Rainforests, World Bank Environment 1 (1992).
66. Congo Basin Forests Partnership (CBFP). Les Forêts du Bassin du Congo-Etat des foret. Kinshasa, Democratic Republic of Congo. (2006).
67. Ministry of Economy and Finance (MINEFI). *Audit Économique Et Financier Du Secteur Forestier Au Cameroun-Draft No 1-Août 2006* (Ministère de l'Economie et des finances (MINEFI), Yaounde, 2006).
68. Alemagi, D. & Kozak, A. Illegal logging in cameroon: causes and the path forward. *For. Policy Econ.* **12**, 554–561. https://doi.org/10.1016/j.forpol.2010.07.008 (2010).
69. Boussema, S. B. F., Allouche, F. K., Ajmi, R., Chaabane, B. & Gad, A. A. Assessing and monitoring the effects of land cover changes in biodiversity. Case study: mediterranean coastal region, sousse, Tunisia. *Egypt. J. Remote Sens. Space Sci.* **26**, 185–196. https://doi.org/10.1016/j.ejrs.2023.01.002 (2023).
70. Coulter Lloyd, L. et al. Classification and assessment of land cover and land use change in Southern Ghana using dense stacks of Landsat 7 ETM + imagery. *Remote Sens. Environ.* **184**, 396–409. https://doi.org/10.1016/j.rse.2016.07.016 (2016).
71. Bunyangha, J., Majaliwa, M. J. G., Muthumbi, A. W., Gichuki, N. N. & Egeru, A. Past and future land use/land cover changes from multi-temporal Landsat imagery in Mpologoma catchment, Eastern Uganda. *Egypt. J. Remote Sens. Space Sci.* **24**, 675–685. https://doi.org/10.1016/j.ejrs.2021.02.003 (2021).
72. Kusiima, S. K. et al. Anthropogenic induced land use/cover change dynamics of Budongo-Bugoma landscape in the albertine region, Uganda. *Egypt. J. Remote Sens. Space Sci.* **25**, 639–649. https://doi.org/10.1016/j.ejrs.2022.05.001 (2022).
73. Bekere, J., Senbeta, F. & Gelaw, A. Analyze of Spatial extent and current condition of land use land cover dynamics for the period 1990–2020 Wayu-Tuka district, Western Ethiopia. *Heliyon* **9**, e18587. https://doi.org/10.1016/j.heliyon.2023.e18587 (2023).
74. Obodai, J., Adjei, K. A., Odai, S. N. & Lumor, M. Land use/land cover dynamics using Landsat data in a gold mining basin-the ankobra, Ghana. *Remote Sens. Applications: Soc. Environ.* **13**, 247–256. https://doi.org/10.1016/j.rsase.2018.10.007 (2019).
75. Fahmy, A. H., Abdelfatah, M. A. & El-Fiky, G. Investigating land use land cover changes and their effects on land surface temperature and urban heat Islands in Sharqiyah governorate, Egypt. *Egypt. J. Remote Sens. Space Sci.* **26**, 293–306. https://doi.org/10.1016/j.ejrs.2023.04.001 (2023).
76. Darem, A. A., Alhashmi, A. A., Almadani, A. M., Alanazi, A. K. & Sutantra, G. A. Development of a map for land use and land cover classification of the Northern border region using remote sensing and GIS. *Egypt. J. Remote Sens. Space Sci.* **26**, 341–350. https://doi.org/10.1016/j.ejrs.2023.04.005 (2023).
77. Thakkar, A. K., Desai, V. R., Patel, A. & Potdar, M. B. Post-classification corrections in improving the classification of Land Use/Land Cover of arid region using RS and GIS: The case of Arjuni watershed, Gujarat, India. The Egyptian Journal of Remote Sensing and Space Sciences xxx, xxx–xx; (2016). https://doi.org/10.1016/j.ejrs.2016.11.006
78. Baidoo, R. & Obeng, K. Evaluating the impact of land use and land cover changes on forest ecosystem service values using landsat dataset in the Atwima Nwabiagya North, *Ghana. Heliyon* **9**, e21736 ; https://doi.org/10.1016/j.heliyon.2023.e21736 (2023).
79. McFeeters, S. K. The use of the normalized difference water index (NDWI) in the delineation of open water features. *Int. J. Remote Sens.* **17**, 1425–1432. https://doi.org/10.1080/01431169608948714 (1996).
80. Tucker, J. C. Red and photographic infrared l, Lnear combinations for monitoring vegetation. *Remote Sens. Environ.* **8** https://doi.org/10.1016/0034-4257(79)90013-0 (1979).
81. Zha, Y., Gao, J. & Ni, S. Use of normalized difference Built-up index in automatically mapping urban areas from TM imagery. *Int. J. Remote Sens.* **24**, 583–594. https://doi.org/10.1080/01431160304987 (2003).
82. Manandhar, R., Odeh, I. O. A. & Ancev, T. Improving the Accuracy of Land Use and Land Cover Classification of Landsat Data Using Post-Classification Enhancement. *Remote Sens.* **1**, 330–344 ; https://doi.org/10.3390/rs1030330 (2009).
83. Rwanga, S. S. & Ndambuki, J. M. Accuracy assessment of land use/land cover classification using remote sensing and GIS. *Int. J. Geosci.* **8**, 611–622. https://doi.org/10.4236/ijg.2017.84033 (2017).
84. Garai, D. & Narayana, A. C. Land use/land cover changes in the mining area of Godavari coal fields of Southern India. *Egypt. J. Remote Sens. Space Sci.* **21**, 375–381. https://doi.org/10.1016/j.ejrs.2018.01.002 (2018).
85. Audry, S. et al. The multiscale tropical catchments critical zone observatory M-TROPICS dataset I: the Nyong river basin, Cameroon. *Hydrol. Process.* **35**, e14138. https://doi.org/10.1002/hyp.14138 (2021).
86. Multiscale TROPIcal CatchmentS (M-TROPICS). Hydrological data, Nyong, Cameroon. URL: (2023). https://doi.org/10.6096/BVET.CMR.HYDRO, accessed March 01.
87. Multiscale TROPIcal CatchmentS (M-TROPICS). Hydrochemical data, Nyong, Cameroon. URL: (2023). https://doi.org/10.6096/BVET.CMR.HCHEM, accessed March 01.
88. Lloyd, J. W. & Heathcote, J. A. *Natural Inorganic Hydrochemistry in Relation To Groundwater an Introduction* (Clarendon Press, Oxford University, 1985).
89. Bureau Central des Recensements et des Etudes de Population (BUCREP). Premier recensement général de La population et de l'habitat du Cameroun. *IV – Tome* **07**, 341 (1976).
90. Bureau Central des Recensements et des Etudes de Population (BUCREP). Deuxième recensement général de La population et de l'habitat du Cameroun. *IV – Tome* **07**, 232 (1987).
91. Bureau Central des Recensements et des Etudes de Population (BUCREP). Troisième recensement général de La population et de l'habitat du Cameroun. *IV – Tome* **07**, 282 (2005).

92. Harris, I., Osborn, T. J., Jones, P. & Lister, D. Version 4 of the CRU TS monthly high-resolution gridded multivariate climate dataset. Sci Data 7, 109; (2020). https://doi.org/10.1038/s41597-020-0453-3 (2020).
93. Multiscale TROPIcal CatchmentS (M-TROPICS). Meteorological data, Nyong, Cameroon. URL: (2023). https://doi.org/10.6096/BVET.CMR.METEO, accessed March 01.
94. Walling, D. E. & Webb, B. W. The reliability of suspended sediment load data. *Int. Association Hydrol. Sci. Publication*. **133**, 177–194 (1981).
95. Pettitt, A. N. A non-parametric approach to the change point problem. *J. Appl. Stat.* **28**, 126–135. https://doi.org/10.2307/2346729 (1979).
96. Mann, H. B. Non-parametric test against trend. *Econometrica* **13**, 245–259. https://doi.org/10.2307/1907187 (1945).
97. Sen, P. K. Estimates of the regression coefficient based on kendall's Tau. *J. Am. Stat. Assoc.* **63**, 324, 1379. https://doi.org/10.2307/2285891 (1968).
98. Kendall, M. G. Rank Correlation Methods, 4th edition. Charles Griffin,London, UK (1975).
99. Yue, S. & Wang, C. Y. The Mann-Kendall test modified by effective sample size to detect trend in serially correlated hydrological series. *Water Resour. Manage.* **18**, 3, 201–218. https://doi.org/10.1023/B:WARM.0000043140.61082.60 (2004).
100. World Bank Group (WBG). Terres agricoles (% du territoire) – Cameroon. URL: https://donnees.banquemondiale.org/indicator/AG.LND.AGRI.ZS?locations=CM&name_desc=false, accessed September 04, 2024.
101. World Bank Group (WBG). Terres agricoles (km carrés) – Cameroon. URL: https://donnees.banquemondiale.org/indicator/AG.LND.AGRI.K2?locations=CM&name_desc=false, accessed September 04, 2024.
102. World Bank Group (WBG). World Development Indicators: Deforestation and biodiversity. URL: (2024). https://wdi.worldbank.org/table/3.4, accessed September 04.
103. Tchindjang, M. et al. Appui au Zonage agricole dans la Région administrative du Centre Cameroun. Conférence OSFACO: Des images satellites pour la gestion durable des territoires en Afrique, Cotonou, Bénin. hal-02189570 (2019).
104. Komba, D. E. et al. Chemical weathering and CO2 consumption in the upper Nyong basin rivers (Central Africa): Insights on climatic and anthropogenic forcing in humid tropical environments. *Sci. Total Environ.* **937**, 173405. https://doi.org/10.1016/j.scitotenv.2024.173405 (2024).
105. Tyukavina, A. et al. Congo basin forest loss dominated by increasing smallholder clearing. *Sci. Adv.* **4**, eaat2993. https://doi.org/10.1126/sciadv.aat2993 (2018).
106. Li, S. & Bush, R. T. Changing fluxes of carbon and other solutes from the Mekong river. *Sci. Rep.* **5**, 16005. https://doi.org/10.1038/srep16005 (2015).
107. Redfield, A. C., Ketchum, B. H. & Richards, F. A. The influence of organisms on the composition of seawater. In *The Sea, 2, Interscience Publishers* (ed. Hill, M. N.) 26–77 (John Wiley, 1963).
108. Tchiadjé Tchouaffé, N. F., Tchotsoua, M., Fonteh, M. & Tchamba, M. Ecological engineering to mitigate eutrophication in the flooding zone of the river nyong, Cameroon. In *Handbook of Climate Change Management* (eds Luetz, J. M. & Ayal, D.) (Springer, 2021). https://doi.org/10.1007/978-3-030-57281-5_8.
109. Wang, F., Wang, Y., Zhang, J., Xu, H. & Wei, X. Human impact on the historical change of CO_2 degassing flux in river Changjiang. *Geochem. Trans.* **8**, 7. https://doi.org/10.1186/1467-4866-8-7 (2007).
110. Raymond, P. A., Oh, N. H. & Turner, R. E. Whitney broussard, W. Anthropogenically enhanced fluxes of water and carbon from the Mississippi river. *Nature* **451**, 449–452. https://doi.org/10.1038/nature06505 (2008).
111. Tadjoung, P. et al. M. N. Economie sociale et solidaire, alternative à l'exploitation anarchique des ressources biologiques du fleuve Nyong de Abong-Mbang à Mbalmayo au Cameroun. (2016).
112. Delač, D., Kisić, I., Zgorelec, Ž., Perčin, A. & Pereira, P. Slash-pile burning impacts on the quality of runoff waters in a mediterranean environment (Croatia). *Catena* **218**, 106559. https://doi.org/10.1016/j.catena.2022.106559 (2022).
113. Audry, S. et al. Contribution of forest fire Ash and plant litter decay on stream dissolved composition in a sub-humid tropical watershed (Mule hole. *South. India) Chem. Geol.* **372**, 144–161. https://doi.org/10.1016/j.chemgeo.2014.02.016 (2014).
114. Feller, M. C. & Kimmins, J. P. Effects of clearcutting and Slash burning on streamwater chemistry and watershed nutrient budgets in Southwestern British Columbia. *Water Resour. Res.* **20**, 29–40. https://doi.org/10.1029/WR020i001p00029 (1984).
115. Li, S. et al. Major element chemistry in the upper Yangtze river: a case study of the Longchuanjiang river. *Geomorphology* **129**, 29–42. https://doi.org/10.1016/j.geomorph.2011.01.010 (2011).
116. Das, A., Chung, C. H. & You, C. F. Disproportionately high rates of sulfide oxidation from mountainous river basins of Taiwan orogeny: sulfur isotope evidence. *Geophys. Res. Lett.* **39**, L12404. https://doi.org/10.1029/2012GL051549 (2012).

Acknowledgements

This work was made possible thanks to a 30-year hydrochemical and hydrological database, provided by Multiscale TROPIcal CatchmentS (M-TROPICS) Critical Zone Observatory (CZO). Thus, authors gratefully acknowledge the M-TROPICS CZO as well as its financial institutions and partners, namely, the Institut de Recherche pour le Développement (IRD), the Centre National de la Recherche Scientifique (CNRS) and the Institut National des Sciences de l'Univers (CNRS-INSU), the Université de Toulouse and its Observatoire Midi-Pyrénées (UT-OMP), and the Institute of Geological and Mining Research– Research Centre for Water and Climate Change (IRGM-CRECC) of Yaounde (Cameroon).

Author contributions

D.E.K. performed the study conception and design, wrote the first draft of the manuscript text and prepared all the figures and tables. Material preparation, data collection and analysis were performed by S.A., J.R., C.L., B.N.N., H.A.B., J.R.N.N., J.J.B. and G.R.N.N. All authors commented on previous versions of the manuscript. All authors read and approved the final manuscript.

Funding

The dataset used in the present study was produced (sample collection and analysis, data validation) through funding by the Institut de Recherche pour le Développement (IRD), by the Centre National de la Recherche Scientifique and its Institut National des Sciences de l'Univers (CNRS-INSU), by the Université de Toulouse and its Observatoire Midi-Pyrénées department (UPS-OMP).

Declarations

Competing interests

The authors declare no competing interests.

Additional information

Supplementary Information The online version contains supplementary material available at https://doi.org/10.1038/s41598-025-11578-7.

Correspondence and requests for materials should be addressed to D.E.K. or S.A.

Reprints and permissions information is available at www.nature.com/reprints.

Publisher's note Springer Nature remains neutral with regard to jurisdictional claims in published maps and institutional affiliations.